Vibrational Spectroscopy in the Detection of Cancer

Rina K. Dukor
Vysis, Inc., Downers Grove, IL, USA

1 INTRODUCTION

Cancer. As human beings we all dread to hear this word from our family members, friends or colleagues. We associate it with death. Yet, as intellectual people, we know that early diagnosis and treatment increase the chances of survival and full recovery. And as scientists, we have an internal desire to help, to help with all aspects of this dreadful disease – early diagnosis, prognosis and treatment. As vibrational spectroscopists we think and want to believe that this form of spectroscopy can be useful. And why should we not?

1.1 Vibrational spectroscopy – sensitivity to structures of biological molecules

A human body, on a simple level, is composed primarily of water, proteins, nucleic acids, lipids and carbohydrates. Any changes in the body leading to diseases such as cancer are thought to be due to some biochemical changes in one or all of these components. And if vibrational spectra are sensitive to the structure of these components, then they too must change with the diseased state. Since the pioneering work of Elliott and Ambrose[1] in 1950 for proteins and Blout and Fields[2] in 1949 for nucleic acids, infrared (IR) and Raman spectroscopies have in fact been shown to be very sensitive to the conformation of these biological building blocks.[3–9]

1.1.1 Nucleic acids

Although all biomolecules are important, the nucleic acids RNA and DNA are especially important because they carry within their structure the hereditary information that determines the identity and structure of proteins. Each protein, unique in its structure and hence in its function, then participates in the processes that characterize the individuality of the cell. In the 50 years since Blout and Field reported the first IR spectra of nucleic acids,[2] IR has been used in applications such as conformational transitions, identification of base composition, effect of base pairing, and DNA–ligand interaction studies. It has also been used in industry for the quality control of products based on DNA, such as fluorescence probes. Figure 1 shows IR absorption spectra of (Figure 1a) calf thymus DNA and (Figure 1b) RNA from calf liver, measured in water in transmission mode (left panel), and as solids using a single-reflection diamond attenuated total reflection (ATR) accessory (right panel). Comparison of the left and right panels leads to a conclusion that these spectra are highly dependent on the state of hydration. The bands with the strongest intensity correspond to regions and assignments of the following vibrations. The 1750–1620 cm^{-1} region corresponds to in-plane double-bond vibrations of the bases. The spectra in this region are very sensitive to base-pairing interactions and base-stacking effects, i.e. effects of hydrogen bond formation. The 1230 cm^{-1} and 1090 cm^{-1} bands are assigned to antisymmetric and symmetric phosphate stretching vibrations, respectively. Ribose has a strong C–O band at 1120 cm^{-1}, marked by a star in Figure 1(b), left panel, which serves as a marker band for RNA in solution. In the solid, the most significant difference between the two nucleic acids is the ratio of intensity of the bands in the multiplet around 1055 cm^{-1}. Raman spectroscopy provides information related to individual nucleotides only. (See **Vibrational Spectroscopy of Nucleic Acids** for more discussion about the vibrational spectroscopy of nucleic acids.)

1.1.2 Proteins

It is a fundamental belief of structural biology that protein function or dysfunction is related to its structure or change

© John Wiley & Sons Ltd, 2002.

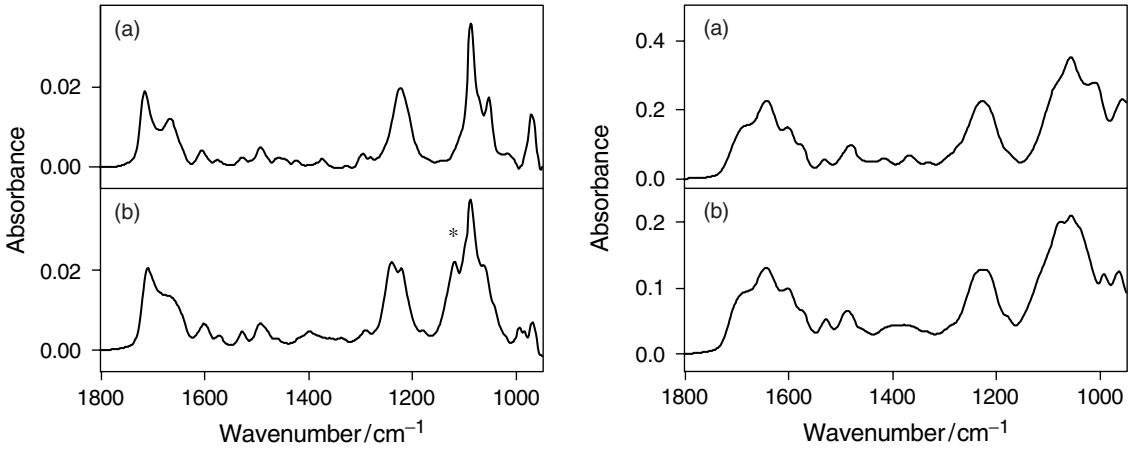

Figure 1. IR spectra of (a) DNA and (b) RNA in water (left panel) and as solid (right panel).

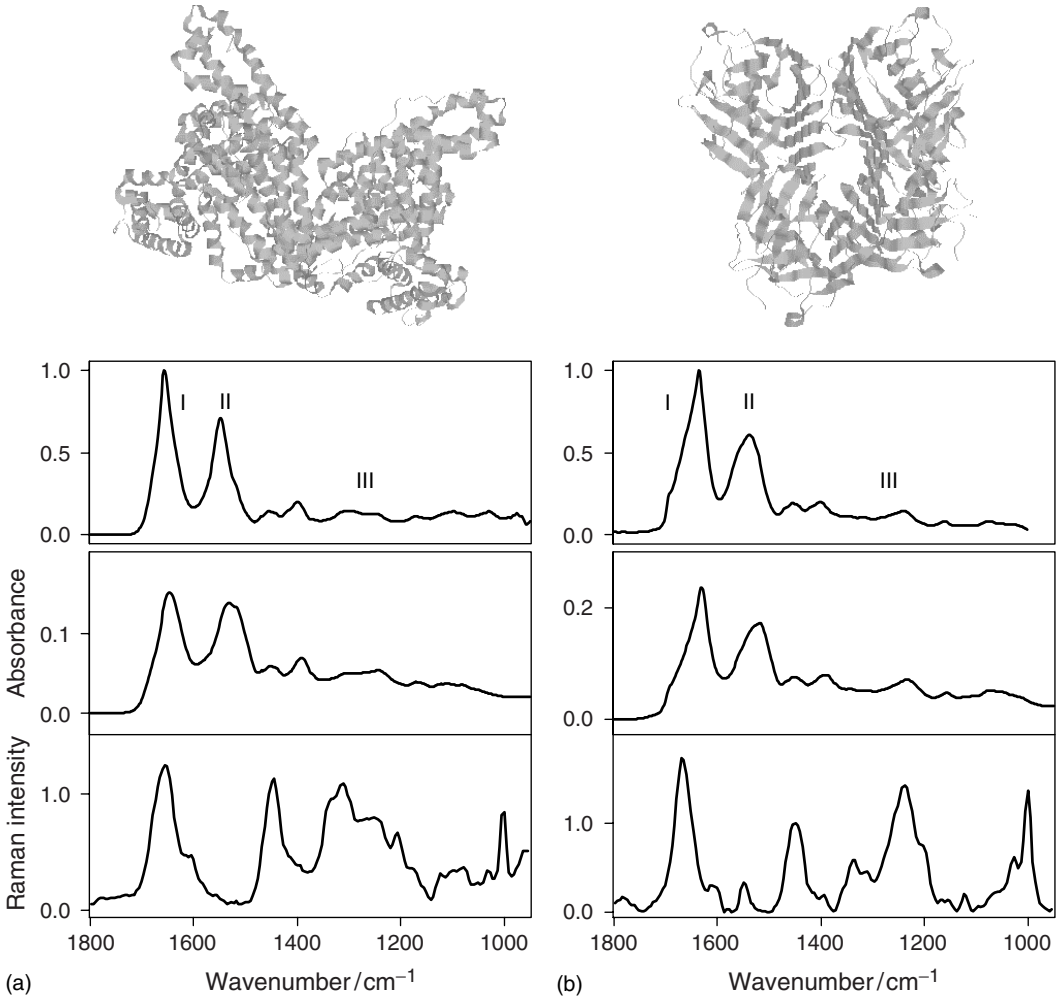

Figure 2. IR spectra in solution (top), solid (middle) and Raman spectra in solution (bottom) of proteins with different secondary structures: (a) albumin; (b) concanavalin A. For solution spectra, proteins are measured in buffered water at concentration of approximately 2% for IR measurements and in 0.1 M phosphate buffer at concentration of 5% for Raman measurements. IR spectra of solutions are normalized to Amide I intensity of 1.0 for ease of comparison. Amide I, II and III modes are marked as such on the spectra.

in structure. Both IR and Raman provide information on the secondary structure of proteins, ligand interactions and folding. Other articles in this handbook (see **Infrared Spectroscopy of Proteins** and **Raman Spectroscopy of Proteins**) address these topics in more detail. As an example of the sensitivity of vibrational spectroscopy to protein conformation, Figure 2 shows the mid-infrared spectra (top and middle) and the Raman spectra (bottom) of two proteins with very different conformations: albumin, whose structure is almost all helical, and concanavalin A, a β-sheet rich protein (no helix and ~40% sheet). In the vibrational spectra, the amide bonds of proteins form so-called chromophores that give rise to nine strong characteristic bands that are named amide A, amide B and amides I–VII. Among these bands, amide I, which is due mostly to the C=O stretching vibrations of the peptide backbone, is by far the best characterized. It gives rise to an IR band in the 1600–1700 cm^{-1} region and has been used the most for structural studies due to its high sensitivity to small changes in molecular geometry and hydrogen bonding of the peptide group. The amide II band, due largely to a coupling of CN stretching and in-plane bending of the N–H group, is extremely weak in the Raman effect. And although it is fairly strong in the IR, giving rise to a band in the 1480–1575 cm^{-1} region, the amide II band is not often used for structural studies per se because it is less sensitive and is subject to interference from absorption bands of amino acid side-chain vibrations. The amide III band, arising from coupling of C–N stretching and N–H bending, and giving rise to bands in the 1230–1300 cm^{-1} region, is fairly weak in the IR but quite strong in Raman but can also be mixed with vibrations of side-chains. In addition to secondary structure information, Raman can provide insight on dihedral angles of C–S–S–C bonds and C–C–S–S bonds and their related conformers; it can also determine how tyrosines are hydrogen-bonded and whether tryptophan residues are in a hydrophobic or hydrophilic environment.

1.1.3 Lipids

Lipids are critical to all biological media by forming the cell walls that keep biological media organized in their necessary compartments. Lipids of various kinds also help regulate the flow of needed biological molecules from one side of a lipid barrier to the other, often assisted by imbedded proteins that form the passages for these molecules called channels. The IR spectrum of a typical lipid is shown in Figure 3. The major absorption bands are at 1738, 1465, 1255, 1168, 1095 and 1057, and 968 cm^{-1}. Lipids and biomembranes are discussed in more detail in **Vibrational Spectroscopy of Lipids** and **Vibrational Spectroscopy of Membranes**, respectively.

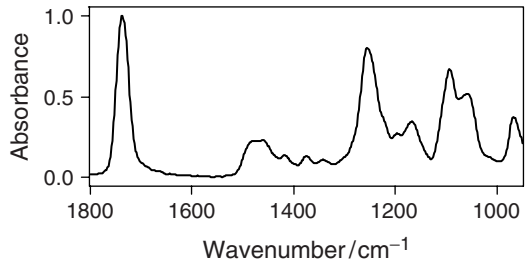

Figure 3. IR spectrum of a lipid.

1.1.4 Carbohydrates

The most common carbohydrates are sugars, or saccharides. Sugars are present in biological media primarily as hexose sugars, such as glucose, where they are an immediate energy source. Pentose sugars are also present, mainly as the ribose component of the nucleic acid backbone of DNA and RNA, both as the component monomers and the much longer polymers, as well as in the energy-transducing oligomeric pieces. Polysaccharides in the body are found either in a free state or combined with proteins, in a complex known as glycoproteins. The only polysaccharide in the body that is not bound to a protein is glycogen. Figure 4 shows a Fourier transform infrared (FT-IR) spectrum of glycogen dissolved in water (a) and as a solid (b). The major absorption bands for solution spectrum are observed at 1153, 1105, 1082, 1043, 1025, 996 (weak shoulder) and 931 cm^{-1}. The corresponding bands for the solid spectrum are 1149, 1078, 1043 (weak shoulder), 1016, 996 and 931 cm^{-1}. Comparison of the two spectra leads to a conclusion that these spectra are highly dependent on the degree of hydration. More specific discussion on carbohydrates can be found in **Vibrational Spectroscopy of Carbohydrates and Glycoconjugates**.

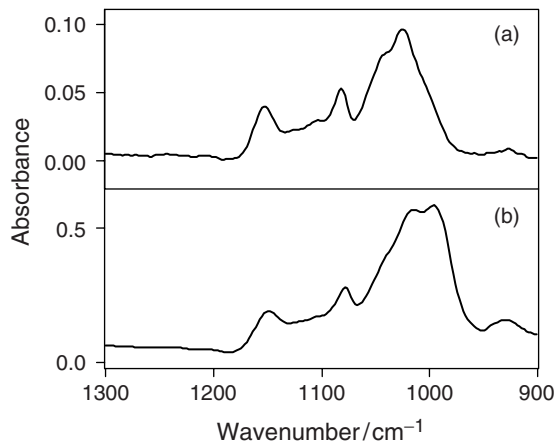

Figure 4. IR spectrum of glycogen dissolved in water (a) and as solid (b). Both spectra are measured with a single-reflection diamond ATR accessory.

1.2 Cells and tissues

1.2.1 Cell biology

We have now established that vibrational spectroscopy is a sensitive tool for studying isolated biomolecules. But is it enough to "detect cancer" or any other disease? And how do we do the experiment? What method do we use? Before we can answer these questions we need to take a step back and understand what it is we are looking at. In fact, as we will show later, it is absolutely critical to understand the biology of the sample before proceeding with spectroscopy.

The basic unit of life is the cell. The essence of a cell is to grow and divide to produce daughter cells, which are likewise capable of generating new cellular molecules and replicating themselves. Cells were first seen over 300 years ago, shortly after the construction of the first microscope. Cells are very small, with diameters much less than 1 mm, so they are invisible to the naked eye. In all eukaryotic (nucleus-containing) cells the inner cellular mass is partitioned into a membrane-bounded, spherical body called the nucleus and an outer surrounding cytoplasm. Cellular DNA is located in the nucleus in the form of rods known as chromosomes. Cells are chemically very sophisticated – even the simplest cells contain about 1000 different molecules. These molecules include various sugars, amino acids, fatty acids, proteins and nucleic acids. There are over 200 different types of cells in the human body,[10] such as heart cells, muscle cells, liver cells, retina cells, red and white blood cells. These cells are assembled into four types of tissue: epithelial, connective, muscular and nerve. Most tissues contain a mixture of cell types. Epithelial tissues are composed of closely aggregated polyhedral cells with very little intercellular substance. These epithelial cells form coherent cell sheets that line the inner and outer surfaces of the body. Connective tissue is characterized by the abundance of intercellular material produced by its cells. This material is composed mostly of a network of tough protein fibers, collagen and elastin, embedded in polysaccharide gel. Connective tissue contains several types of cells, each having its own morphological and functional characteristics. The most common cell found in connective tissue is fibroblast. Nerve tissue is found all over the body as a communication network. Nerve tissue consists of nerve cells or neurons and several types of glial cells or neuroglia, which support neurons. Muscular tissues can be divided into three main types, skeletal, smooth and cardiac, each composed of cells with different function and appearance. The four tissues, in association with one another and in variable proportions, form different organs and systems of the body.

1.2.2 Cancer

Cancer is the leading cause of death in the western world. It is the number one cause of death for women in the United States and if the decline in heart disease mortality continues at the present rate, then cancer will soon be the leading cause of death in the United States and many European countries. Over 1 million cases of cancer occur in the United States every year, excluding curable skin cancers, which add another 700 000 cases annually. The highest mortality rates are seen with lung, female breast, prostate and colorectal cancers. Over 500 000 people die of cancer each year in the United States alone. Over 8 million Americans alive today have had some type of cancer. About half are considered cured. And for the grimmest statistic of all: about one in three people now living in the US will develop some type of cancer. The good news is that more people are being cured and the 5-year survival rate is at an all time high of 59%.[11]

Cancer is not a new disease. Hippocrates reported to have distinguished benign from malignant growths. He introduced the term "karkinos", from which the word "carcinoma" is derived. Cancer is a complex family of diseases, and carcinogenesis – the turning of a normal cell into a cancer cell – is a complex multi-step process. Figure 5 shows a simplified diagram of cancer progression. Anyone interested in applying spectroscopic techniques to the study of cancer is strongly encouraged to educate themselves further by reading textbooks on pathology and cancer biology. In a simple description, tumor (or neoplasm, which means "new growth") begins when some cell within a normal population sustains a mutation that increases its propensity to proliferate when it would normally rest, shown in Figure 5(a). The altered cell and its daughters look normal but they grow and divide too much. This condition is termed *hyperplasia* (Figure 5b). After some time, which could be years, one of these cells suffers another mutation that further loosens control on cell growth. This cell proliferates very fast and the offspring of this cell appears abnormal in shape and orientation, as shown in Figure 5(c). This state is known as *dysplasia*. Again, after some time, a mutation occurs that alters cell behavior. The affected cells become even more abnormal in growth and appearance. If the tumor is contained within original tissue, it is called in-situ cancer (Figure 5d). This tumor may remain contained indefinitely but often the cells acquire additional mutations, continue to grow and divide and invade underlying tissue. At this point the mass is considered to have become malignant (Figure 5e). If cells break away from such a tumor, they can travel through the blood stream or the lymph system to other areas of the body and establish new tumors. They continue to grow in new locations. The spread of a tumor to a new site is called *metastasis*. These

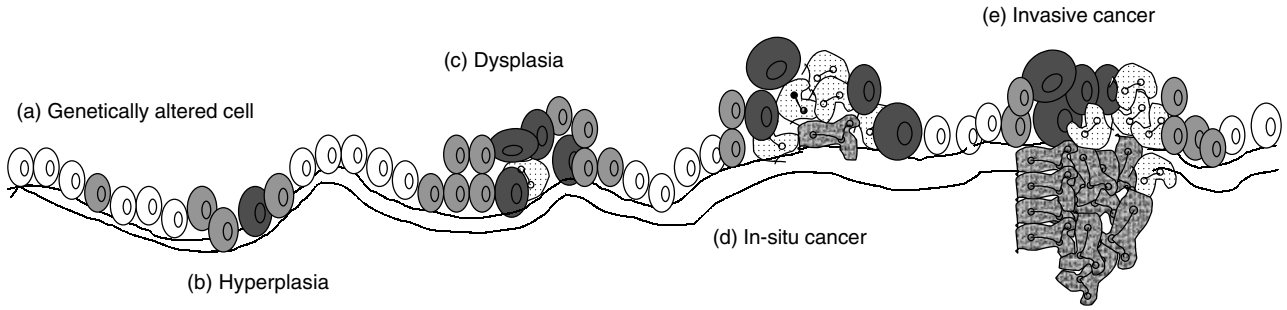

Figure 5. Simplified diagram of cancer progression. (a) Normal cells with a single genetically altered cell, (b) hyperplasia, (c) dysplasia, (d) in-situ cancer and (e) invasive cancer.

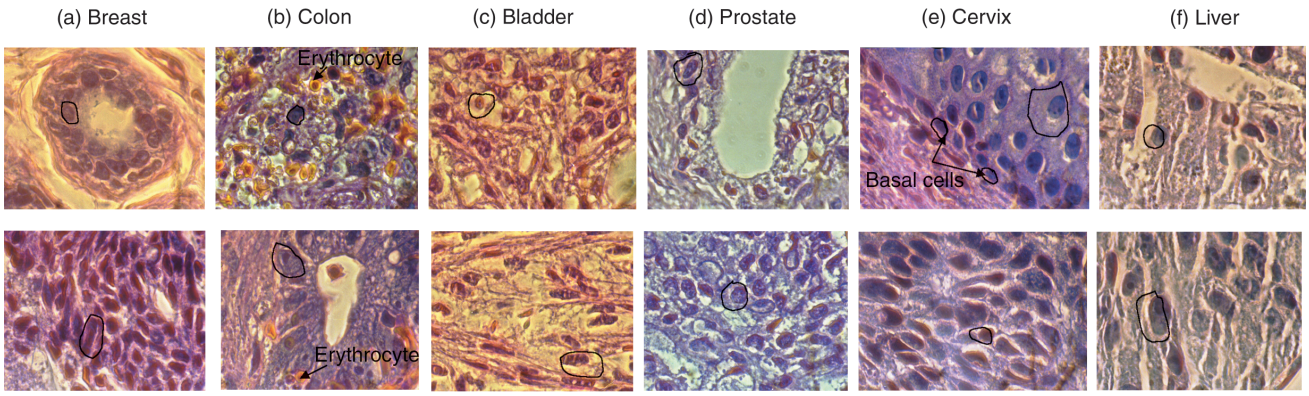

Figure 6. Image of normal (top row) and malignant (bottom row) cells from tissue biopsy of the following organs: (a) breast; (b) colon; (c) bladder; (d) prostate; (e) cervix; and (f) liver. Magnification × 100. Individual cells are circled.

tumors may become lethal by disrupting the function of a vital organ. Tumors are of two basic types: benign and malignant. By definition, benign tumors do not invade adjacent tissue borders nor do they metastasize to other sites. The primary descriptor of any tumor is its cell or tissue of origin. Most human malignancies arise from epithelial tissue and are called carcinomas.

The "gold standard" in most cancer diagnostics is microscopic evaluation, by a pathologist, of a stained tissue obtained from biopsy of a particular organ (this procedure is called pathologic histology or histopathology). Figure 6 shows a microscopic image of such biopsies. The top row is comprised of images of normal cells and the bottom row of images of malignant cells from biopsies of the following organs, all taken under the same magnification: (a) breast; (b) colon; (c) bladder; (d) prostate; (e) cervix; and (f) liver. Although these cells are from different tissues, the differences between "malignant" and "normal" have many observations in common and include the following:

- The morphology and size of cells that are different and more variable than those of normal cells.
- The nucleus of a cell that is larger than the nucleus of a normal cell.
- The appearance of large cells with multiple nuclei.
- The invasion of normal tissue by a neoplasm.

The diagnosis of disease and tumor staging is thus in the hands of a pathologist. This diagnosis will lead to a decision by an oncologist regarding the type of cancer treatment to be employed. Although many pathologists are exceptionally good at what they do, this analysis is somewhat subjective. As one pathologist said: "You don't know what you see – you see what you know". "Misdiagnosis", with a false negative rate of 20% and an unknown true false-positive rate, is especially common in screening of cervical cancer, such as evaluation of pap-smears. Additionally, in some cases (about 10%), a pathologic examination may not produce a firm diagnosis, either because certain tumors are histologically similar or because cells are so poorly differentiated that their tissue of origin cannot be determined. In these cases, other diagnostic procedures might be useful and include, but are not limited to, electron microscopy, immunohistochemistry, cytogenetics, and levels of various tumor markers in the patient's serum or urine – and maybe someday vibrational spectroscopy.

2 EXPERIMENTAL TECHNIQUES

Tissues are very heterogeneous, comprising several components and different cell types. Different cells have intrinsically different size and shapes, as can be seen from

Figure 6 (top row). Normal breast cells, for example, are about 10 μm in diameter, with a nucleus of about 5 μm, whereas cervical cells range from 10 to 50 μm in diameter, with a nucleus of 10–5 μm depending on the layer of cells. If normal breast tissue was measured with a beam size of 30 μm, the resulting absorbance at each wavenumber would be a weighted average of the absorbance resulting from the cell itself, including the nucleus and cytoplasm, basement membrane plus some other components surrounding the cell, such as connective tissue or fat. If, however, the sample were a cervical tissue, or a cervical smear composed mainly of superficial layer of cells, and an individual cell was centered under the IR beam, the resulting spectrum would be only of a nucleus plus some cytoplasm of a cervical cell. It should therefore become immediately clear that one design of an experiment would not satisfy a study of tissues or cells from different organs. *Experiments must be designed after careful consideration is given to the nature of the sample and after much thought about the component of interest – cells, nuclei, basement membrane, connective tissue, fat or an average of all*. Choosing the right sampling technique is probably the most critical decision and one that is most often ignored. Consideration must be given to the original state of the sample and its stability. Varieties of sampling techniques are available for IR and Raman spectroscopies and all have been covered elsewhere in this Handbook. They will be described here briefly in relation to the sample itself.

2.1 Histological samples

A sample that a pathologist evaluates to diagnose cancer is most often a piece of a tissue from biopsy that has been fixed, sectioned, mounted on a glass slide and stained. A cover slip is placed for protection and the tissue is evaluated under a light microscope. Fixation makes cells permeable to stains and preserves the tissue's physical structure. The procedure usually involves brief immersion of a tissue into formaldehyde solution (formalin) or an alcohol/water mixture, although the latter is now rarely used. Formaldehyde is known to react with the amine group of tissue amino acids and it promotes coagulation, not precipitation of proteins. After fixation tissues are usually embedded in a liquid wax, such as paraffin, that permeates and surrounds the tissue. (Water is first extracted by dipping the tissue in a graded series of ethanol/water mixtures, and then by bathing in xylene or benzene.) This embedding medium is then hardened to a solid block by cooling. The tissues are cut into thin slices with a microtome (similar to a meat slicer). Each slice is then laid flat on the surface of a glass microscope slide. The thickness of slices is usually on the order of 3–8 μm thick. Prior to staining the tissue, the embedding medium is removed by dipping the tissue in a solution of Hemo-De, a mixture of d-limonene and butylated hydroxanisole. Appropriate stains are then applied. These stains have preference for a particular part of the cell – the nucleus or membrane. Hematoxylin, the dye of choice for most solid tumors, has an affinity for negatively charged molecules and therefore reveals the distribution of DNA and RNA in a cell.[12] A combination of dyes, hematoxylin and eosin (H&E), is most commonly used, and stains the nucleus in dark blue, cytoplasm in pale pink and collagen (in connective tissue) pink. Any fixation and embedding procedure has a danger that the treatment may distort the structure of the cell. Immersion of tissues in lipid solvents, such as xylene, dissolves the tissue lipids. An alternative method of preparation that lessens this danger is rapid freezing, which precludes either fixation or embedding. The frozen tissue can be cut directly with a cryostat. Although frozen tissues have an advantage that they represent a more native form of the tissue, they are more difficult to prepare, and the presence of ice crystals causes many morphological details to be lost.

Since tissue samples prepared for histology are readily available, it would be natural to think of using them for vibrational spectroscopic studies. But many problems come to mind right away: glass absorbs mid-infrared radiation; what effects do paraffin and dye have on the spectra? Most investigators choose to make fresh samples for spectroscopy, while using histological sample as a reference, and study them with a variety of sampling accessories available. We will come back to use of histological samples for spectroscopy after discussion of sampling accessories.

2.2 IR and Raman sampling techniques

One of the big advantages of vibrational spectroscopy, especially IR, is that it is not limited to a particular state of the sample. Spectra can be obtained from liquids, solids (pellets, powders, films, tissues), slurries and suspensions. In principle, Raman has an intrinsic advantage over IR for liquid biological samples, due mostly to the weak scattering of water. To that effect, a significant proportion of IR applications to-date have concentrated on the in-vitro studies of tissues and cells, whereas in Raman spectroscopy the big push is toward the in-vivo diagnostics. In Raman spectroscopy, excitation of light can be either ultraviolet (UV) ($\lambda < 400$ nm), visible ($400 \leq \lambda \leq 700$ nm) or near-infrared ($\lambda > 700$ nm). Different tissue types and samples require optimization of excitation wavelengths.[13] For example, tissues exhibit strong fluorescence, due to the presence of cellular components, that can obscure the tissue Raman

spectra when visible excitation is used. Since fluorescence decreases rapidly at longer excitation wavelengths, near-infrared excitation is now used in a majority of biomedical studies. Near-infrared light penetrates tissues deeply, on the order of millimeters. Alternatively, it is possible to use UV light at wavelengths below 270 nm to circumvent the fluorescence interference problem. With UV resonance excitation, the tissue penetration depth is on the order of micrometers, so this technique is good for surface layers. One does have to be careful with tissue damage when using UV light. Visible excitation Raman spectroscopy appears to be best suited for in-situ cell studies because of lower fluorescence of individual cells compared with tissues.

So in some ways, Raman spectroscopy is "more complicated" experimentally than IR. But the two techniques are complementary, each having advantages and disadvantages. Not surprisingly, spectroscopists seem to have their technique of choice and find samples or problems appropriately. But for a medically trained person interested in "using" vibrational spectroscopy, the decision is not straightforward and primarily should depend on the sample and question of interest. Neither technique has regulatory approval nor is commercially available for routine medical diagnostics, but significant leaps have been made toward this goal. Over the last decade, dramatic technological advances have occurred for many components of vibrational spectroscopic instruments including introduction of microscopes, new multi-channel detectors, tunable diode lasers, and optical fibers. We provide below a survey of available sampling methods for IR and Raman and subdivide this section into liquid and solid sampling techniques and additionally describe in detail the differences between macroscopic, microscopic and fiber-optic detection for solid samples like tissues, the backbone of cancer diagnostics.

2.2.1 Liquid sampling

Blood and urine (liquid samples) are generally used in medicine for diagnostics and screening of different diseases, including cancer, but no one to our knowledge has used these matrices directly for cancer studies with vibrational spectroscopy. One type of cancer, leukemia, involves the blood-forming lineage of cells. So blood could be a component of choice for the study of this disease. And urine, for example, could be used for bladder cancer studies. Studies in the mid-infrared are often done on isolated cells that are dried[14] or on dried whole blood or blood serum samples. Shaw *et al.*[15] and independently Werner *et al.*[16] used blood samples for distinguishing healthy versus diseased patients with the mid-infrared light, but none of the diseases or analytes studied were cancer related. Blood is also used for glucose monitoring in the near-infrared region, as described in **Glucose Measurements by Vibrational Spectroscopy** in this volume of the Handbook, and in Raman spectroscopy.[13,17] Berger *et al.* used whole blood and blood serum to measure Raman spectra with near-infrared excitation, but again the analytes were not specifically cancer-related.[17]

In general, the simplest way to measure biological fluids in the IR is by using transmission techniques, that is by passing the IR beam directly through the sample, and in the Raman by using nonresonance Raman scattering. For mid-infrared studies, 5–15 μL of sample is placed on IR transparent windows, such as CaF_2 or BaF_2, separated by a thin spacer. Since most biological fluids contain a significant amount of water and because water absorbs strongly in the mid-infrared region, the spacer needs to be thin in order to keep the water absorbance below one. Usually, this corresponds to a thickness (pathlength) of less than 10 μm. New IR cells have recently become available that do not use a physical spacer. In such a cell one window is etched to a desired thickness, say 6 μm, and the second flat window is placed on top.[18,19] This design eases placements of sample onto the cell, making it very convenient for study of water based samples. Other methods of "liquid" sampling by transmission include placing a small amount of liquid on an IR disposable card or by drying the fluid onto IR transparent substrates.[20] In both cases, water is dried off, resulting in a film. Although these methods seem to have the advantage that water is removed and thus its strong interfering bands, Jackson and Mantsch warn of several possible problems associated with the drying process such as formation of heterogeneous films.[21]

Viscous liquid samples can be analyzed in the IR using the ATR technique.[22] Other articles explain the technique in more detail (see **Standard Sampling Techniques for Infrared Spectroscopy** and **Macro and Micro Internal Reflection Accessories**). In short, the heart of an ATR accessory is a crystal of IR transparent material of high refractive index, for example zinc selenide (ZnSe) or germanium (Ge), also called the internal reflection element (IRE). When IR light hits the IRE at a proper angle of incidence, the radiation undergoes total internal reflection. Inside the IRE a standing wave of radiation is established, called an evanescent wave, that does not terminate at the crystal surface but penetrates a little beyond the surface. When the sample is brought into contact with the crystal, it can interact with the evanescent wave and absorb IR radiation, resulting in detection of its IR spectrum. The name attenuated total reflection is given because the evanescent wave is attenuated by the sample's absorption. One word of caution for ATR studies: both liquid and solid material can adsorb onto the surface of the ATR crystal, and thereby interact with it.

Alternatively, the near-infrared region of the spectrum can be used for study of liquid biological samples. Observed absorption bands in this region arise from overtones and combinations of C–H, N–H and O–H vibrations. These spectra are often broader and less featured than the corresponding mid-infrared spectra of fundamental modes, which also means more delocalized information content. Overtone and combination bands are weaker than their fundamental counterparts, requiring use of longer pathlength cells, on the order of 0.1–1.0 mm. The main advantage of near-infrared measurements is that samples can be measured in glass containers, such as blood collected in a test tube, and analysis is totally nondestructive. Additional discussion on studies of liquid sampling of biological fluids in the IR can be found in another article (see **Pathology by Infrared and Raman Spectroscopy**) in this volume of the Handbook.

Although water absorbs strongly in the IR, it is a weak scatterer in the Raman, giving Raman an advantage for measurements of biological fluids. But not all fluids can be measured with all available excitations. For example, analysis of intact blood is not possible with visible excitation because the main component of blood is the protein hemoglobin, and the associated heme group has strong absorption bands in the 400–520 nm region. Dilution of blood with a buffer or use of near-infrared excitation can overcome this. Raman spectra with near-infrared excitation at 830 nm have been successfully measured for whole blood and blood serum.[17] One potential source of problems with the use of high intensity lasers is heating of the sample, which can lead to damage of cells. In the work of Berger *et al.*,[17] laser intensity of 250 mW was focused into a spot approximately 50 μm in diameter. The effect of laser heat was lowered, but not eliminated, by the use of a magnetically driven rotating cylindrical pellet that was placed inside the sample cuvette.

2.2.2 Solid sampling

Blood, urine and other biofluids present very intriguing samples for cancer detection because they would involve a standard simple test without a need for biopsies. Unfortunately, these matrices are too complex for vibrational spectroscopy especially as pertains to early cancer detection. If vibrational spectroscopy is ever to be accepted by the medical community as a tool for diagnosis, we must correlate, at least initially, our studies to an accepted gold standard – tissue biopsies or cell smears. That means that we must do our studies on the same samples – tissues, extracted cells or cell smears, depending on the organ or cancer of interest. Most studies to date, beginning with the first IR measurements of tissues in 1949 by Blout and Mellors,[23] have been done on many variations of sample preparation, including full microtome thin sections,[24–51] homogenized or pulverized tissues,[52–54] cell smears or pellets,[26,55–68] extracted cells from tissues,[69] whole cells either cultured or isolated from blood[70–72] or DNA isolated from cells.[73–78] The obvious question is "what is the best way to analyze tissues and cells?" There does not seem to be consensus in the literature on this question, but the trend does seem to go, at least by the number of papers published in the last four years, toward microscopy, in both IR and Raman spectroscopies. But even with microscopy, a variety of experimental conditions can be set that affect the final results. This section is divided into "macroscopic" and "microscopic" measurements, implying the size of the focus point on the sample, in millimeters or micrometers, respectively, and not necessarily the use of a microscope.

Macroscopic sampling. In most commercial FT-IR spectrometers, the diameter of the beam at the focus point is at least a few millimeters. This means that the sample area measured, even if cell windows decrease the beam size, is at least a few square *millimeters*! In Raman, the spot size can be smaller and is typically on the order of 1 mm in diameter. From our earlier discussion of composition of cells and tissues and from Figure 6, this means that the spectra measured in macro mode are an *average* of all cellular and extracellular components present in the path of the beam. Individual components have distinct vibrational signatures and the resulting spectra are dependent on the contribution of each component and its concentration. Because different components are *always* present in different concentrations throughout microtome tissues, even within the same tissue slice, spectra obtained in this mode will definitely show differences. These differences could be significantly larger within the same group of tissues, say normal, than for a different type of tissue, say malignant. On the other hand, the presence or absence of a particular component in significant amounts might indicate "malignancy" or change towards malignancy, and that can be easily detected by a macroscopic method.

IR transmission and reflection The simplest way to measure solids, as it is with liquids, is by using transmission techniques. Solid samples, such as films or thin tissues, can be simply placed between two IR transparent windows. It is important to keep the thickness of the film between 1 and 20 μm, so the sample does not block all the light. Many early studies of tissues, frozen or fixed, were made in this manner. Alternatively, the sample can be mixed with an inert KBr matrix to form what is known as a KBr pellet. An important requirement is to grind both the sample and KBr powder to reduce the particle size to less than 3 μm. KBr

pellets are often used in the study of cells and cell pellets, and homogenized and pulverized tissues. Early studies of tissues from the Wong group were done with a diamond anvil cell and pressure tuning.[26–30] A diamond anvil cell consists of two small diamonds with very flat faces that are mounted parallel to each other. The sample is placed on one diamond, and the second is brought into contact with the first, flattening the sample. Screws on the outside holder can be used to adjust the pressure. Cells of this type have been described in the article by Polsky and van Valkenburg (see **The Diamond Anvil Cell**).

In reflection sampling techniques, the IR beam is reflected off the surface of the sample instead of passing through the sample as is done in transmission. Several reflection techniques exist, and are defined depending on the angle of incidence and angle of reflection. The angle of incidence is defined as the angle the incoming light makes with the surface normal, where the surface normal is a line perpendicular to the surface of the sample. The angle of reflection is defined as the angle the outgoing light makes with the surface normal. There are two different types of reflection – specular and diffuse. Specular reflection occurs when the angle of incidence equals the angle of reflection. Diffuse reflection occurs when the angle of incidence is fixed, but the angles of reflection vary. A form of specular reflection, called transflection or double-transmission, is often used for tissue studies. This form requires a smooth surface that is a mirror, which has a coating that is strongly reflective of IR radiation. Typically gold substrates are used. Thin slices of tissue, 1–10 μm, are placed on the mirror substrate, the light beam passes through the sample to the substrate, reflects off the surface of the mirror, and passes through the sample a second time. It is also possible to study tissues and cells on a glass slide with the use of an ATR accessory. For a single-reflection IRE, the spot size is on the order of 100–200 μm. This technique is very easy and fast for a single spot on the sample, but it does not allow for tissue mapping because motorized xy-stages are not available.

Fiber-optic probes A fiber-optic probe coupled to an IR[79–81] or Raman[82–87] spectrometer provides an intriguing and very promising possibility of in-vivo, real-time spectroscopic diagnostics. Many applications can be envisioned, such as immediate diagnosis of skin cancer in the doctor's office and spectroscopy guided biopsies, where optical fiber is incorporated into needles, endoscopes and catheters. In the IR, fiber-optic probes can be operated in transmission or an ATR mode, with the latter being most common. The principle is fairly simple – the beam is directed through an optical fiber to the ATR crystal and back to the spectrometer through another optical fiber. An advantage of such measurement is practically no sample preparation, noninvasiveness of the procedure, very fast turnaround time for diagnosis and little expense. The area measured is the area of contact between crystal and sample and is usually a few square centimeters. McCreery's and Puppels's groups pioneered use of Raman fiber-optic probes in conjunction with core needle biopsy (McCreery) and through endoscopes and laparoscopes (Puppels). Different applications will demand different probes and several designs have been described in the literature.[82,85–88] The usual construction of a fiber-optic probe is to have one laser fiber surrounded by a number of collection fibers, normally 6 or 7. Such an array is then embedded in a biopsy needle or inserted through the endoscope. One other advantage of Raman fiber-optic probes is that they can reduce power density at the sample significantly.

Raman spectroscopy The initial Raman spectra of tissues were measured with visible laser excitation, primarily with argon ion lasers, but the spectra were masked by fluorescence.[89] Introduction of FT-Raman spectrometers, using 1064 nm excitation (Nd : YAG lasers) and cooled InGaAs or Ge detectors allowed collection of fluorescence-free spectra of tissues. However, InGaAs or Ge detectors exhibit substantial noise so the collection time needed to obtain spectra of tissues with good signal-to-noise ratio (S/N) was on the order of 30–60 min.[90–92] Excitation using a diode laser near 800 nm has been found to be the optimum trade-off between loss of Raman intensity as $1/\lambda^4$ for the excitation wavelength and the greatly reduced fluorescence available further into the near-infrared region. The development of diode lasers and low-noise cooled silicon charge-coupled device (CCD) cameras sensitive in the near-infrared, combined with the use of dispersive systems instead of FT-based spectrometers, has enabled the measurement of fluorescence-free tissue Raman spectra on a much faster timescale,[83,84,87,93–96] in minutes, even seconds. The use of diode lasers and dispersive systems has provided better sensitivity and the possibility of f-number matching of spectrographs with optical fibers for better throughput. The spot size is dependent on the optics used and because most research groups build their own systems or modify existing commercial systems, this number varies but is on the average around 1 mm. These three general components, near-infrared laser excitation, dispersive spectrograph and CCD cameras, are now used for most tissue studies, in vivo or in vitro, and as with IR spectrometers can be easily modified for microscopic studies by an addition of a microscope.

Microscopic sampling. Microscopy is an integral part of diagnostics, with visible microscopy of stained tissues considered a gold standard. Coupling of a microscope to an FT-IR or Raman spectrometer provides a very powerful

technique of measuring vibrational spectra of individual morphological components of tissues. We have shown above that different biomolecules have very distinct IR and Raman spectra, and we have also discussed earlier the composition of cells and tissues. It should then come as no surprise that vibrational spectroscopy can create spectral maps of tissues, which if given some color notation, would correspond directly to tissue histology. In addition to providing a color to which most pathologists are accustomed, these maps also provide fairly detailed biochemical information not available from other techniques. It is important to re-emphasize that these maps are produced from spectra without any prior knowledge of tissue architecture on samples that are not stained. Spectral mapping allows for *combined* understanding of morphology and biochemistry that gives rise to observed spectra. In our opinion, it is important to understand the spectral features of *each* morphological structure. By comparing spectra of each individual structure in the normal tissue and diseased state we can begin to understand how these components change during the process of carcinogenesis.

But as we saw earlier in Figure 6, individual components of tissues have intrinsically different sizes and the same components vary in size depending on the tissue of origin. So, unless components are measured with the beam size or spot size corresponding to the dimensions of that component, again, even with the microscope, the resulting spectrum will correspond to a composite spectrum of several such components, weighted with respect to their relative concentrations. And although many maps published in the literature grossly correspond to stained tissues, "pure" representative spectra derived from such maps are not necessarily those of real "pure tissue components". We find this after a survey of the current literature and write this not as criticism but as our opinion and suggestion for future work. We feel it is very important to carefully study stained tissues with light microscopy to understand the intricate details of tissue morphology before proceeding with spectroscopy in order to determine the spot size desired. Therefore, in order to set up experiments correctly, it is important to understand the factors that affect spatial resolution in vibrational microspectroscopy.

IR microspectroscopy has been described in detail in a separate article (see **Mid-infrared Transmission Microspectroscopy**) and in many excellent reviews, including those by Messerschmidt[97,98] and Reffner and Martoglio.[99] Specifically, pathology by IR and Raman, and biopsy-microscopy imaging are covered elsewhere in the Handbook (see **Pathology by Infrared and Raman Spectroscopy** and **Ex Vivo Vibrational Spectroscopy Imaging** and have been recently discussed by Jackson and Mantsch[21] and Wetzel and LeVine.[100] Raman microspectroscopy instrumentation is reviewed in separate articles (see **Raman Microscopy** and **Raman Imaging**).

In microspectroscopy, one of the most important and difficult steps is to define accurately the sample area, or measured area, especially if the sample of interest is very small such as a single cell or a cluster of cells embedded in tissue. While it is quite easy to establish the sample area by viewing it with visible radiation, the actual area that is analyzed is larger for IR radiation because of the larger diffraction limit in this region and the fact that the diffraction limit increases linearly with wavelength. Messerschmidt defines spatial resolution as the "ability to measure the spectrum from an object delineated by the apertures without significant impurity radiation from neighboring objects".[98] Neighboring objects to cells in tissues could be among many possible constituents of other cells, either malignant or normal, connective tissue matrix, or fat lobules. In his review, Messerschmidt provides an excellent example of sample area definition in the IR. This is an attractive example because it imitates a typical tissue but with a known two-component matrix. The example consists of an acrylic fiber 20 μm in diameter that is embedded in polystyrene and then cross-sectioned to a 10-μm thickness. Three spectra were recorded, all with the same spectrometer conditions and for the same length of time. In the first spectrum, no aperture was set to eliminate the embedding medium. In the second, one variable aperture was used to delineate the fiber. In the third spectrum, two apertures were used, one in the focal plane of the objective and one in the focal plane of the condenser, both delineating the same area of the sample. The first spectrum had the best S/N but was predominantly a spectrum of the embedding medium polystyrene. The second spectrum was mostly the spectrum of fiber with little contamination from polystyrene. And the third spectrum, although with the worst S/N, was attributed to fiber only. From this example, one might conclude that setting the aperture(s) small enough to match precisely the object of interest is all that is needed. But how low can the aperture be set? Decreasing the aperture dimensions leads to degradation of S/N and more importantly, as the aperture size approaches the wavelength of light, diffraction becomes a serious limitation. The diffraction limited spatial resolution or least resolvable separation (LRS) is defined as ($0.61\lambda/NA$), where λ is the wavelength of the energy and NA is the numerical aperture of the optical system.[98] (The diameter of the diffraction ring, known as the Airy disk, is taken as $1.22\lambda/NA$. The resolving power is the smallest distance between two objects, so the radius of the Airy disk is used.)[101] The NA is equal to the product of the refractive index of the medium outside the lens (objective or a condenser) and the sine of half the angle that the marginal

ray from the lens makes with the optical axis of the lens and thus ranges theoretically from 0 to 1.0 in air.[101] Most IR microscope objectives have NAs in the range of 0.5–0.7. Using the above formula, the diffraction limited spatial resolution in the 1700–1000 cm^{-1} region is on the order of 5–12 μm, with higher resolution (lower number) at higher NA. These values represent the absolute minimum spot size achievable with a given objective. But because some radiation falls outside the defined spot, the real sample area is much higher, especially at longer wavelengths, where it could be as high as three times the minimum spot size.

Commercial microscopes fall into two major categories: systems with high NAs with one area-defining aperture and systems with medium NAs with two apertures (confocal microscopes). Both designs lead to improvement in spatial resolution. NA also affects throughput, so it should be as large as is practical. Magnification of the microscope does not affect throughput or diffraction limit and in all commercial systems a choice of 15× or 32× magnification is provided, mainly in order to allow convenient visualization and masking of the sample.[98] In theory, 32× magnification should provide higher-resolved minimal spot size, but that is true only if NA increases significantly, which is not the case with commercial objectives. The NA in the most popular microscope systems from Thermo Spectra-Tech (Shelton, CT, USA) for a 15× objective is 0.58, and for a 32× objective it is 0.65. For design reasons, the pupil in a 32× objective is smaller than in a 15× objective. In the use of Spectra-Tech objectives, when the NA stays practically the same and the magnification changes, the light is vignetted so extra magnification provides no increase in spatial resolution.[102] In addition, vignetting decreases the signal intensity because some light rays no longer make it to the detector.

Why is it necessary to worry about the diffraction-limited spatial resolution and the dimensions of the sample area detected? Because of our firm belief that in order to understand if vibrational spectroscopy can be used for the detection of cancer it is important to first understand the spectral features of *pure individual* components of tissues, cells and maybe even subcellular components before drawing further conclusions. At Vysis, we have concentrated on studies of breast tissues and, as shown in Figure 6, the normal breast cells are about 10 μm in diameter – right on the limit of average diffraction-limited spatial resolution in the mid-infrared region! To achieve this spatial resolution, the aperture must be set very low, resulting in fairly low noisy spectra. Two technological breakthroughs now allow for the detection of IR spectra at the diffraction limit with good S/N – the use of synchrotron radiation and the detection with focal-plane array (FPA) technology. These advances are discussed in the following sections.

Regardless of the source or the detection system used, all commercial microscopes coupled to an FT-IR spectrometer can be operated in three modes – transmission, external reflection, and internal reflection with the use of an ATR objective. The basic descriptions and requirements for these three techniques were discussed earlier. An ATR objective is particularly suitable for studies of tissues for two reasons. First, this is the only technique that allows measurements of samples mounted on standard glass slides.[43] Many samples are archived on glass slides and thus are readily available. This technique is nondestructive meaning, that the same sample can be used for other analyses, such as a pathologist's evaluation, fluorescence-in-situ-hybridization or DNA extraction. Glass is a strong absorber in the mid-infrared region and thus is not suitable for transmission studies. However, with an ATR objective, the depth of penetration of light is typically on the order of 0.5–3.5 μm and since the tissue section thickness is usually 4 μm and above, the light never reaches the glass substrate. In addition, ATR can lead to demagnification effects. An IRE is a hemispherical lens so the beam cross-sectional area of the radiation passing through is demagnified by the square of the refractive index of the IRE.[99] For example, for a hemispherical Si IRE with a refractive index of 3.4, a 100 × 100 μm effective aperture will actually interrogate a ~30 × 30 μm area measured at the sample.

One other point of clarification is needed with respect to nomenclature in microspectroscopy. In all commercial microscopes intended for use with FT-IR spectrometers, an aperture is placed in the beam to define the sampling area. Technically this is a beam stop that allows definition of an area comparable to the diffraction limit or higher, as discussed previously. For a diffraction limit of 10 μm at 1000 cm^{-1}, this area should not be smaller than 150 μm × 150 μm for a 15× objective and 320 μm × 320 μm for a 32× objective. The physical device that is set in every experiment is an aperture and it has a fairly "large" area. Too often in the literature, it is said that the "variable aperture was adjusted to say 50 μm × 50 μm", implying that the sample area measured was 50 × 50 μm, not that the actual physical device was set to 50 μm × 50 μm. If it were the physical device that was set, then the sample area measured would be 3.3 μm × 3.3 μm for a 15× objective, well below the diffraction limit. Perhaps a better and more concise terminology would be to say "the resulting effective aperture was 50 μm × 50 μm",[103] or "measured area was 50 μm × 50 μm" (although in this case, as we have seen above, the exact measured area is not definitive).

Mid-infrared synchrotron radiation Synchrotron IR light is about two to three orders of magnitude brighter than a conventional globar source found in most commercial

mid-infrared FT-IR spectrometers. The high brightness of this source allows setting of microscope apertures corresponding to sample geometrical areas equal to the diffraction limit or even smaller[103,104] with resulting spectra of high S/N. The synchrotron beam size is fairly small, on the order of 300 μm × 600 μm at the National Synchrotron Light Source (NSLS) at Brookhaven National Laboratory, but it can vary for different facilities. After demagnification and use of a 32× objective, the geometric size of the beam is 4 μm high × 8 μm across.[105] If no apertures are used then diffraction-limited spatial resolution depends only on the wavelength of light and NA of the objective, as discussed in the previous section. The NA of the 32× objective used at NSLS is close to 0.65, therefore the diffraction limit is equal to the wavelength. Considering diffraction, the spot size (or full width at half-maximum of the image) is actually 8-μm high and 16-μm wide, the spot size changing with wavelength.[105] Placing an aperture to define a sample area smaller than a wavelength of light is possible but spatial resolution is controlled by diffraction and in reality no increase in spatial resolution is observed.[103] Use of a confocal (dual aperture) microscope helps increase the spatial resolution by 30%[103] due to "suppressed diffraction rings" because of better sharpness and better contrast.[105] So using dual-aperture configuration it is possible to measure a spot size of ~5–8 μm with good image contrast in the 1700–1000 cm^{-1} range.

Synchrotron radiation is thus ideal for studies of cells and tissues, because it allows measurement of low noise spectra at the diffraction limit, which matches the size of many individual cells and even nuclei. Spectra have been obtained for a single living cell[106] and cells during the cell cycle and for dying cells.[107] Measurements with synchrotron radiation are not practical for every day medical use in a hospital or clinical laboratory setting, but high quality spectra obtained in these experiments of individual cell and tissue components can help understand the process of disease and basic cell and cancer biology. Additional discussion on synchrotron sources can be found in a separate article (see **Synchrotron and Free Electron Laser Sources of Infrared Radiation**).

Mid-infrared FPA detection Use of an FPA detector in an IR microscope, instead of a single-element detector, makes it possible to analyze a fairly large area of sample with very high spatial resolution. In this detection method, spatial resolution is attained from the individual pixels. Each detector pixel serves as an area-defining aperture, thus the spot size is determined by the dimension of the array. In 1994 Lewis *et al.* carried out the first experiments combining an FPA with a step-scanning interferometer coupled to a reflective IR microscope.[108,109] This approach, now known as hyperspectral imaging, allows for a simultaneous determination of both spatial and spectral information. In the experiment, the interferometer is sequentially stepped and data are acquired from each pixel in the array at each interferometer step. Data from one pixel at all steps are combined to produce an interferogram, which is Fourier transformed to produce the single beam spectrum. This is done for all pixels simultaneously. The result is a three-dimensional block of data, known as an "image cube", that spans one wavelength and two spatial dimensions. This cube can be seen either as a series of spatially resolved spectra, one for each point on the image or as a series of wavelength-resolved images. The first experiments were done using 128 × 128 arrays containing indium antimonide (InSb) elements that are sensitive between 2000 and 10 000 cm^{-1}. More recently, mercury cadmium telluride (MCT) detectors have been introduced, either in a 64 × 64 array or a 256 × 256 array, which opened the way to studies in the mid-infrared region.[110] With the original design at Procter and Gamble, based on the Bio-Rad UMA300A microscope with a focusing lens before a 64 × 64 MCT array and a 15× objective, the field-of-view (FOV) was a square of 800 × 800 μm area, with approximately 12.5 μm per pixel. With the new infinity-corrected optics, the FOV is a 400 × 400 μm area, with an image on each pixel of 6.25 μm. The 256 × 256 array allows an image of an 800 μm × 800 μm square with a pixel image of a little over 3 μm. The image of 6.25 μm per pixel is right on the limit of diffraction for 6 μm wavelength of light, and of course 3 μm is below that limit. As discussed in previous sections, because each pixel is acting as an area-defining aperture, the spot size is limited by diffraction and is equal to approximately 6–10 μm in the region of 1700–1000 cm^{-1}. For array detection, the microscope is not operated in a confocal arrangement (no apertures), so in these experiments there is no gain as is possible in the synchrotron measurements. So, the advantage of using the 256 × 256 arrays is to sample a larger area (800 μm × 800 μm) at the diffraction limit.

One of the advantages of FPA studies is the ability to average spectra from ~6 μm × 6 μm areas, corresponding to individual cells to 800 × 800 μm corresponding to an "average" of tissues, making it equivalent to macroscopic sampling studies. This ability to average spectra from different areas will help answer the question that we will address in Section 3 – what needs to be measured for effective early diagnosis or prognosis of cancer – nuclei, cells, surrounding tissue or an average of all? Further details on instrumentation and data acquisition with FPAs can be found elsewhere (see **Instrumentation for FT-IR Imaging**).

CCD detection in Raman Three basic strategies have evolved for the measurement of microscopic Raman images. The first is the oldest and least efficient of the methods, namely point-by-point collection measured by

translating the sample beneath a fixed small laser focus. The second is to image the laser beam as a line on the sample and to image the line through a dispersive spectrometer to a CCD detector. This allows collection of the Raman spectrum of each point on the line simultaneously. The entire image can be obtained by sweeping the laser line image across the sample in discrete steps. The third, and most efficient, imaging technique, is to image the entire sample area through a tunable optical filter and onto the surface of a CCD detector. The Raman images are then collected at discrete wavelengths. The use of a tunable filter leads to some loss of spectral resolution. The spatial resolution of this method is constrained by the size of the CCD pixels, which are typically 25 μm square. Higher spatial resolution can be achieved by magnification of the image on the CCD up to the diffraction limit, beyond which further magnification yields no more detail. Near-infrared Raman has a larger diffraction limit size (0.7 μm and lower) than the corresponding limit in the visible (0.4–0.7 μm) by the ratio of the wavelengths used in these two regions. Generally, the method of CCD detection is now preferred because of the higher signal quality of CCDs and the freedom of not having to translate the sample spatially to form the image.

2.3 Spectroscopic sample

Preparation of samples for histology, as discussed in Section 2.1, involves mainly five steps: fixation, paraffin embedding, sectioning, mounting on glass slides, and staining. These samples are readily available from any hospital or histology laboratory. Most tissue samples available from tissue banks are stored in paraffin blocks, and in many cases tissues are stored on glass slides for follow-up studies. It would seem natural to want to use these samples for in vitro spectroscopy, but can we use them? Many questions arise regarding how the preparation processes affect the tissue samples and resulting spectra, with fixation, paraffin embedding and staining being the most controversial. When a surgeon takes a biopsy, the sample can be either placed in a jar with formalin or be frozen with liquid nitrogen. At this point, the spectroscopist can choose to use either sample. The problem with frozen tissues is the difficulty in preparation and stability. Microspectroscopy mapping experiments can take several hours, and in that time tissues will degrade. Formalin fixation prevents degradation and preserves a tissue's physical structure. Formalin can be washed off with water or isotonic saline solution. Paraffin has several strong absorption bands in the mid-infrared region, as shown in Figure 7, with the most intense bands at 1472, 1462, 1378 and 1126 cm^{-1}. Many papers make a note of this intense absorption and continue to state that these

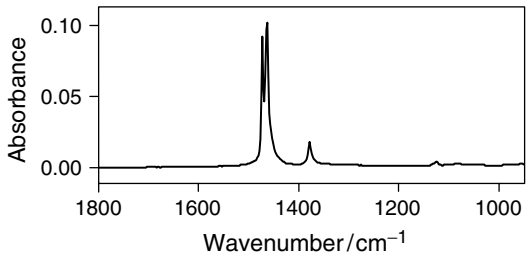

Figure 7. FT-IR absorbance spectrum of paraffin on glass slide, measured with single-reflection diamond ATR accessory.

bands will contaminate the spectra of tissues. The effectiveness of the deparaffinization procedure, i.e. dipping the tissue in Hemo-De solution, can be judged by these intense absorption bands. If the three most intense bands are not observed it is reasonable to conclude that all paraffin has been removed, or, that at least it will be at a low enough concentration that it does not affect the spectroscopy. Shim and Wilson[111] have examined the effects of tissue drying, freezing, thawing and formalin fixation on near-infrared Raman spectra and have concluded that artifacts of preparation are minimal, except for tissue dehydration.

The overwhelming majority of tissue studies have been done on unstained sections, either frozen or after removal of paraffin on previously formalin-fixed and paraffin-embedded sections. Unstained tissues are very homogeneous to the eye, appearing alike throughout the section. Identification of regions of interest is extremely difficult, if not impossible, even with a polarizer in the microscope. The use of unstained tissues is mainly due to the general belief that absorption bands due to the stains interfere with the absorption spectrum of the sample. Figure 8 shows spectra of two breast tissues, as an example of a worst-case scenario

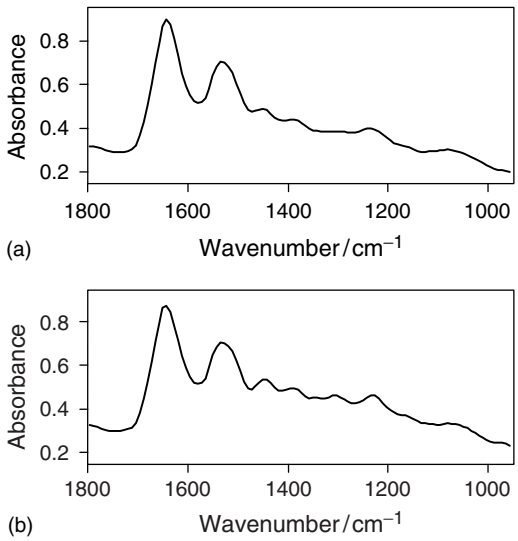

Figure 8. FT-IR absorbance spectra of breast tissue (a) unstained and (b) H&E stained. Spectra are measured using an FPA detection system.

due to heavy staining. The tissues are adjacent slices measured in the same general area with FPA instrumentation, so the spatial resolution is on the order of 12 μm. The IR absorbance spectrum resulting from an unstained section is shown in Figure 8(a) and a spectrum resulting from a section stained with H&E is shown in Figure 8(b). The band at $\sim$1303 cm^{-1}, observed in Figure 8(b) and not seen in 8(a), is thus assigned to the stain. In all further analysis, this spectral region is neglected. The other points of contention for not using stained samples are the possibility of interaction between the stain and different components of the tissue and differences of extent of such interactions, or other possible artifacts that may lead to subtle changes that might be misinterpreted as a disease state.[21] All of these points are very well taken and probably have validity. In our research we make an assumption, which might be proven wrong later, that individual components in all tissues of the same type (epithelial cells, connective tissue) interact, if at all, with the stain similarly. That is the epithelial cells in breast tissue interact the same way in all breast tissues and all connective tissue interacts in a similar manner to that of all breast tissues, and so on.

We believe that for initial studies it is more important to understand and compare spectral features of different tissue components *individually* in the tissue matrix than it is to measure an unknown area and an average of all such components, even if there is some interaction with the stain. We take great efforts to monitor bands that are due to stain. One other point of concern involves washing with ethanol or xylene during the staining process that may lead to delipidation and protein denaturation. This point is certainly a cause for concern but, again, an assumption is made that such effects will be very similar for all tissues. To prove this assumption and to evaluate other differences in sample preparation, we compared tissue slides prepared by three different histopathology laboratories and find no spectral differences that can be seen by the naked eye, that is no formalin, paraffin or stain bands stand out. It is possible that in our imaging studies we do not observe any noticeable differences because we measure individual components of tissues and not averages as is done in almost all other studies. By averaging several components such as cells, connective tissue matrix and fat lobules, as an example, more dramatic differences might be observed. Although we prefer to use stained sections, other groups either stain the spectroscopic sample after measurement or make an additional sample of a stained tissue. In the case of two samples, one usually identifies the area of interest on unstained tissue section by anatomical landmarks as compared to the case for stained tissue. The two slices are adjacent microtomed sections and although they are very similar, they are not identical. This difference is shown in Figure 9 for an image

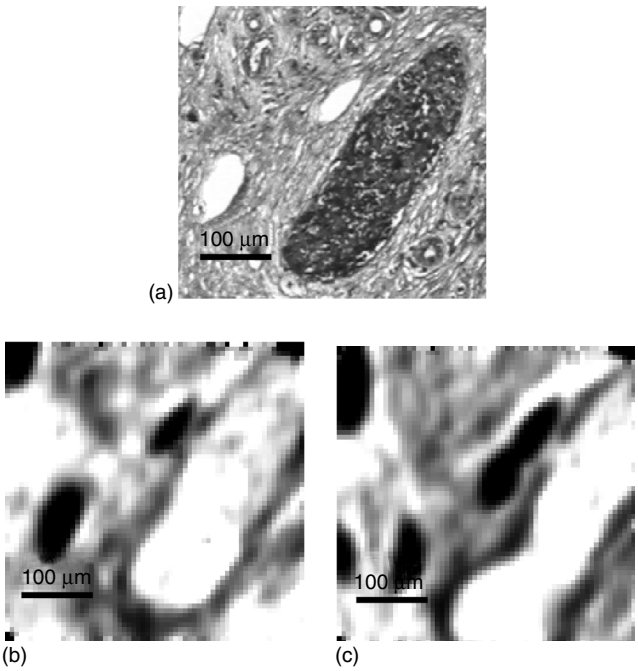

Figure 9. (a) Transmission visible image of an H&E stained malignant breast tissue specimen on an IR reflective slide; (b) IR reflectance image at 1658 cm^{-1} of the same exact sample as in (a); (c) IR reflectance image at 1658 cm^{-1} of an adjacent section of the same specimen in the same area as imaged in (a) and (b).

obtained for two adjacent breast tissue slices. Spatial errors could be easily made that would result in misinterpretation. An analogy could be made to a roll of salami, where each consecutive slice is similar but not identical due to fat and meat variations. With the use of one sample that is stained after spectroscopic analysis, it is difficult to identify a priori areas of interest and, once the sample is stained, spectral measurements cannot be repeated for the same sample.

Glass slides that are used for visible microscopy are very inexpensive and easy to use. But glass absorbs strongly in the mid-infrared and thus does not appear suitable for tissue measurements unless an ATR objective on a microscope or stand-alone ATR accessory is used, as discussed previously. With an ATR objective and Si IRE, the depth of penetration is on the order of 0.5 to 3.5 μm, so the radiation never reaches the glass substrate. Another alternative for measurements on glass slide is to use the near-infrared region. A recent introduction of IR-reflective glass-coated slides by Kevley Technologies (Chesterfield, OH, USA) allows visible examination of stained tissues and IR measurements on the same tissue sample so the spectroscopist and pathologist can evaluate the same specimen. The slides are coated with a thin film that is highly reflective in the IR and transmissive to visible radiation. The IR measurements using this substrate are made in the reflection–absorption mode.

3 APPLICATIONS

Over the last decade, studies using vibrational spectroscopy have been conducted on samples from a variety of organs, including brain,[31,33,34,92,112,113] breast,[32,33,37,42,43,45,47,48,54,73–75,78,83,84,90,114,115] colon,[26,27,30,70,116] cervix,[28,38,40,44,55–68,88,117] endometrium,[36] heart,[35] liver,[41,79,118] lung,[51,52,69] lymph system,[39] prostate,[76] skin[29,46,78,96,119–122] and thyroid.[24] The results of all these studies, on a gross level, can be summarized as follows: "normal and malignant tissues can be differentiated on the order of 80–100% accuracy with the use of some statistical analysis". If in fact this is true, then why isn't a vibrational spectroscopy instrument, either IR or Raman, in clinical trial for use in cancer diagnostics? (As of this writing, to the best of our knowledge, there is no system in clinical trials for cancer diagnosis or screening except possibly for glucose measurements). Is it sufficient to confirm malignancy on a biopsy, even with close to 100% accuracy? Does the world of cancer diagnostics need an "automated" spectral map to replace histology and do these maps help in establishing a diagnosis? Can vibrational spectroscopy really establish early onset of disease or stages of cancer? We will try to address these provocative questions by discussions of several cancers, the state of the art in diagnosis and review of vibrational spectroscopy studies. We cannot review every single paper or cancer studied so we have chosen to concentrate on the cancers for which most vibrational spectroscopy work has been done – breast and cervical cancers. (Skin cancer literature is partially reviewed in **Ex Vivo Vibrational Spectroscopy Imaging**.) Our own research concentrates on breast cancer so most of the discussion will be devoted to this topic, but "potential and pitfalls" that will be pointed out certainly apply to other cancers as well.

In the early 1990s, Wong and colleagues published several papers on the application of IR spectroscopy to study of cancer tissues and cells. This initial work started the field of "IR diagnostics". In the papers published in 1996[59] and 1997,[61] they concluded the following: "Cervical cancer and other cancers studied to date exhibit certain characteristic spectral changes which are the result of the following structural changes at the molecular level:

1. the presence of extensive hydrogen bonding on the phosphodiester groups of nucleic acids;
2. an increase in the symmetric phosphate stretching band of the phosphodiester groups of nucleic acids, indicating tighter packing of nucleic acids;
3. hydrogen bonding of C–OH groups of carbohydrates and proteins are reduced due to phosphorylation of these C–OH groups;
4. the degree of disorder of methylene chains in membrane lipids increases;
5. the methyl to methylene ratio decreases significantly due to hypomethylation;
6. decreased glycogen levels (in glycogen rich tissues)".[61]

And although these studies and many others indicate that IR spectroscopy has a potential to become a powerful tool for detection of malignancies, it soon became apparent that some other factors may contribute to the observed spectral changes, such as nonneoplastic diseases, the presence of other types of cells or mucin, that is, factors that are not due to the process of carcinogenesis.

3.1 Breast

Breast cancer is the most frequently diagnosed cancer, after skin cancer, in women in the United States. It is second only to lung cancer as a cause of cancer-related deaths among women. According to Health and Human Services, about 40 800 women will die from breast cancer this year in the United States alone.

Early detection can save lives. Current methods of screening include a combination of a clinical examination, where a doctor searches for a lump that can be felt, and mammography. Mammography is an X-ray technique that is used to visualize the internal structure of the breast. The signs of malignancy are based on calcifications, architectural distortion and asymmetry. But not all carcinomas can be found with mammography. In fact, mammography fails to detect about 20% of all breast cancers. A new device was approved by the US Food and Drug Administration (FDA) in 1999, T-Scan 2000, intended to be used along with conventional methods. It is a hand-held scan probe that is placed on the breast to evaluate certain suspicious areas detected on the mammogram. The T-Scan images are based on differences in the electrical impedance between malignant tumor tissue and surrounding normal tissue. Other devices in testing are based on digital mammography, magnetic resonance imaging (MRI) and ultrasound. MRI appears to be unique in its ability to define local tumor staging. But both MRI and ultrasound have limitations, since neither can consistently detect microcalcifications or very small tumors. If a lesion is found, a woman undergoes a biopsy, either by surgical removal of a piece of tissue or fine needle aspirations. Eighty percent of women who undergo surgical breast biopsies in the United States do not have cancer. Image-guided needle biopsies, including a possible fiber-optical Raman probe, would offer potential advantages of minimal tissue damage, reduced waiting time for diagnosis and lower costs.

A diagram of the anatomy of a breast (anatomically known as a mammary gland) is shown in Figure 10. The breast is composed of fat, ligaments, glands, milk ducts,

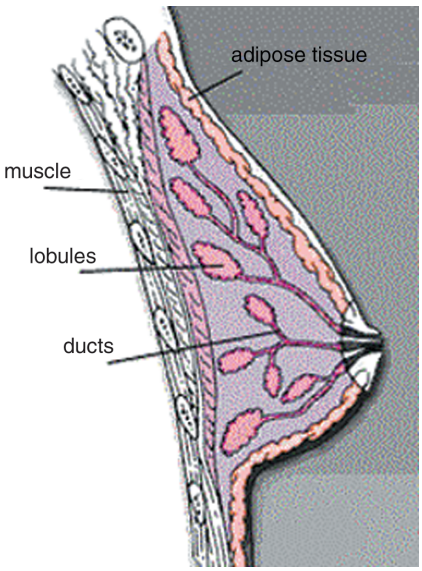

Figure 10. Schematic diagram of a female breast.

blood vessels, lymph channels and nerves. Each adult female breast contains between 15 and 20 compartments called lobes (glands of the breast), each of which is divided into smaller compartments called lobules, which end in dozens of tiny bulbs that can produce milk. The lobes, lobules and bulbs are linked by thin tubes called ducts. All ducts unite to form larger ducts that lead to the nipple. There are 5–12 separate ductal systems in each breast, the function of which is to drain the lobules. The ducts are lined by columnar epithelium resting on a basement membrane that separates it from stromal tissue. The stroma, often referred to as connective tissue, is composed of fatty tissue, fibrous tissue and supporting ligaments. Each breast also contains blood vessels and vessels that carry lymph (a body fluid containing lymphocytes). The lymph vessels lead to small bean-shaped organs called lymph nodes, clusters of which are found under the arm, in the chest and in many other parts of the body. The breast undergoes many changes during a woman's life, both with age (puberty, pregnancy, lactation and menopause) and cycle time (menstrual cycle). These changes are due to hormonal level fluctuations because cells in the breast contain receptors for female hormones, estrogen and progesterone.

A photograph of a biopsy of a normal tissue, taken from a woman who underwent breast reduction mammoplasty is shown in Figure 6(a) (top). Microscopically, a duct often looks like a "flower", either round or elongated. The size of a round duct on the average is about 40–50 μm. The cells are uniform, with clear nuclei in the middle and a little cytoplasm, and are arranged in a circle around the lumen. The size of each cell is about 10–12 μm.

Tissues in any area of the breast can undergo changes that cause diseases, benign or cancer. The most common of the benign breast conditions are fibrocystic changes, benign breast tumors or breast inflammation. Benign breast conditions are very common. According to the American Cancer Society, they can be found in nine out of ten women. Breast cancer is not one disease. There are *12* different types of breast cancer, with the most common being ductal carcinoma, which begins in the lining of the milk ducts. Another common type, lobular carcinoma, begins in the lobules. Carcinomas can be either invasive or noninvasive, the latter called carcinoma in-situ (CIS). Ductal carcinoma in-situ (DCIS) or lobular carcinoma in-situ (LCIS), if not removed, can change over time and become invasive. DCIS, one of the most common types of carcinoma found by early screening with mammography, is characterized microscopically by cells that have cancer-like appearances but without extension across the basement membrane. The cells are large, with prominent nuclei and abundant cytoplasm. Areas of necrosis are often apparent in the lumen of tumorous ducts. Among invasive carcinomas, infiltrating ductal carcinoma is by far the most common form of breast cancer, accounting for as much as 60–80% of malignant tumors. The next most frequent type is infiltrating lobular carcinoma, with 5–14% frequency, followed by medullary (3–4% frequency), mucinous (2–3%) and others. A common occurrence is the combination of different carcinoma subtypes. Carcinomas of the breast can also develop in men, from the epithelial cells of the ducts, but they are observed about 100 times less frequently than in women. In infiltrating ductal carcinoma, the tumor cells can grow in small or large nests and the amount of connective tissue varies considerably. The size of the tumor cells varies – some cells have abundant cytoplasm with large nuclei; but others are small and have small nuclei. Often large nucleoli are observed. Examples of infiltrating ductal carcinoma are seen in Figure 6(a) (bottom) and Figure 11(a). In Figure 11(a), a resemblance of a duct with lumen is still apparent, with cells broken through the basement membrane. Some tumor cells may calcify. This is especially true when the tumor contains large amounts of collagen fibers. And in about 20% of tumors, lymphocytes can infiltrate the breast cancer. Medullary and mucinous breast cancer are shown here as examples of how diverse and different histology of breast cancer can be. Figure 11(b) shows a photograph of a tissue biopsy from medullary carcinoma and Figure 11(c) shows a photograph of a tissue biopsy from mucinous carcinoma. The growth of large tumor cells and an intense lymphocyte infiltration characterize the medullary carcinoma. The tumor cells are large, with an abundant cytoplasm, vesicular nuclei and prominent nucleoli. Numerous tumor cells are also in mitotic division (possessing two nuclei). Mucinous carcinomas, on the other hand, are dominated by the deposits of mucinous material.

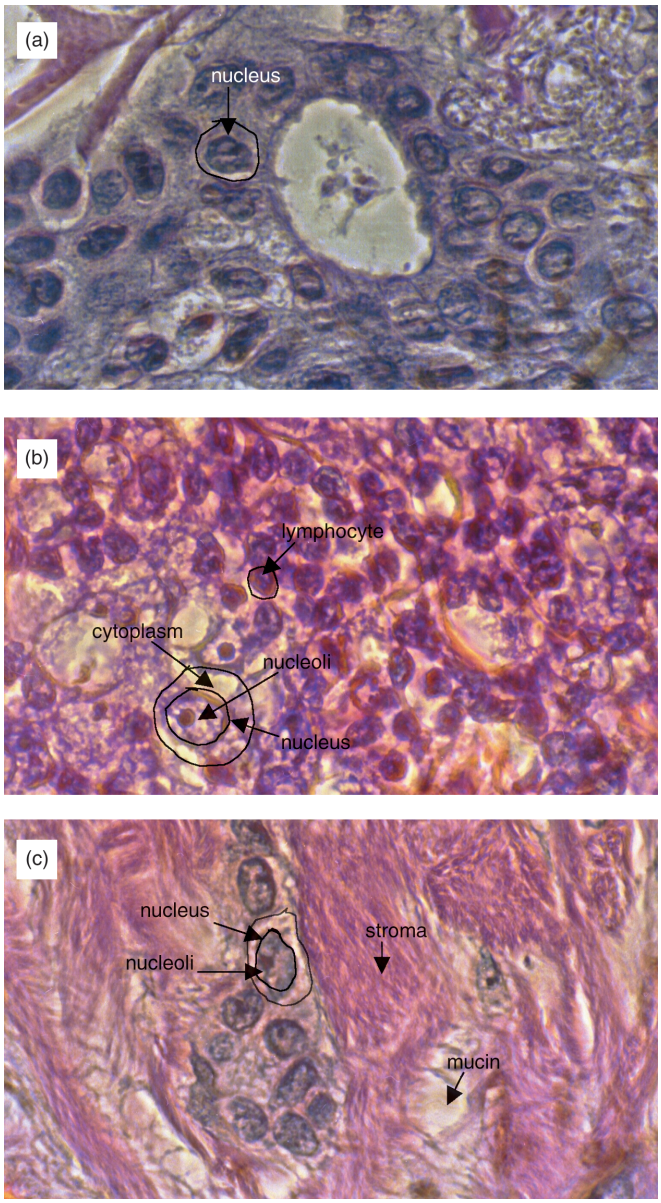

Figure 11. Photograph of tissue biopsy from (a) infiltrating ductal carcinoma, (b) medullary carcinoma, and (c) mucinous carcinoma. Magnification ×100.

The tumor cells are embedded in this material and form only small nests.

Clinical staging of breast cancer is based on the size and extent of the primary tumor, regional lymph node status, and the presence of distant metastases. Prognosis or chance of recovery depends on many factors, including: the type and stage of cancer; lymph node involvement, that is, if cancer has spread to any lymph nodes; hormone receptor status or whether tumors contain receptors for estrogen /progesterone hormones; proliferative capacity of a tumor, i.e. estimation of how fast the tumor is growing; and oncogene activation, that is presence of her-2/neu oncogene.

In 1991, Alfano *et al.*[90] recorded the first Raman spectrum of breast tissue, using 1064-nm excitation and a FT-Raman spectrometer. They analyzed 14 breast tissues (three normal, four benign and seven malignant) and observed that malignant tissues showed only two bands, at 1651 cm^{-1} and 1445 cm^{-1}, out of four that were observed for the normal tissues. Missing were bands at 1300 cm^{-1} and at 1078 cm^{-1}. They also observed that spectra of benign tissue had bands at 1659, 1445 and 1240 cm^{-1}. They concluded that relative intensity of bands at 1651 and 1445 cm^{-1} could be correlated with disease. Redd *et al.*,[114] joined by Frank *et al.*,[83] used several different excitation wavelengths and concluded that spectral differences between benign and malignant tissues, characterized by intensity differences in some peaks, were due to lipids and carotenoids. In a later study, Frank and McCreery[84] compared spectra of normal tissue, benign tissue (fibrocystic disease) and malignant tissue (infiltrating ductal carcinoma). In agreement with Alfano studies, using the area ratio of 1654/1439 cm^{-1} bands, they were able to differentiate between malignant and normal tissue. They also noted a shift in frequency from 1439 cm^{-1} in normal tissue to 1450 cm^{-1} in infiltrating ductal carcinoma. However, they were unable to differentiate between carcinoma and fibrocystic disease. The latest studies on breast tissues with Raman come from Feld's group. Feld's group uses three approaches: in-vitro macroscopic, microscopic and development of in-vivo diagnostic techniques that include design of a needle probe. Manoharan *et al.*[115] collected data from 61 specimens taken from 13 patients (15 normal, 15 benign and 31 malignant) using a macroscopic Raman system with an excitation wavelength of 830 nm, 80 mW laser power and sampling a 1-mm diameter spot size. Consistent with previous studies of Alfano, and Frank and McCreery discussed above, it was found that normal tissue spectra were dominated by Raman bands of fatty acids (1657, 1442 and 1300 cm^{-1}), while the Raman spectra of benign and malignant tissue were dominated by protein bands (1667, 1452, 1260, 890 and 820 cm^{-1}). Using principal component analysis (PCA), 14 of 15 normal, 13 of 15 benign, and 31 of 31 malignant samples were "correctly diagnosed". No false negatives were determined and 2 of 15 benign samples were misclassified.

In 1995, two important papers were published by Mantsch's group,[32,33] describing measurements of breast tissues and breast cells using FT-IR spectroscopy. Both papers discuss composition of tissues and "contamination" of IR spectra because of absorption by the connective tissue protein, collagen. They emphasize that great care must be exercised in obtaining spectra of tissues and a requirement for an extensive understanding of tissue pathology. The paper by Jackson and colleagues[32] puts forward

a hypothesis that previously reported changes observed between malignant and normal tissues, in a variety of organs, and attributed to structural changes in DNA, may have an alternative explanation and may in fact be due to the amount of stromal content. They strengthen their hypothesis by presenting a spectrum of a breast tissue from an invasive ductal carcinoma tumor, whose composition was approximately 60% invasive epithelial cells and 40% stroma. Comparison of this spectrum to that of collagen led to the conclusion that the majority of bands can be attributed to collagen absorption bands. It is important to note that FT-IR measurements were carried out in a macroscopic transmission mode, either using a diamond anvil cell or a pair of CaF_2 windows. The second paper by Fabian *et al.*[33] compares FT-IR spectra of a suspension of tumor cells, tissues from human breast tumors and tissues from xenograft tumors (transplanted tumors grown in mice). Tissues were measured in a macroscopic transmission mode and using a microscope, sampling an area of $30\,\mu m^2$. Comparison of the spectra of human tumor and xenograft tumor, collected in a macro mode, reveal differences in the increased intensity of the shoulder at $1635\,cm^{-1}$ and peaks at 1340, 1283, 1240, 1205 and $1033\,cm^{-1}$ bands in the spectrum of the human tumor. Again, these spectral changes are attributed to differences in collagen content, since stromal content of xenografts is expected to be reduced as compared to human tumors due to the pattern of growth. Microscopic measurements of $30\,\mu m^2$ areas of tissues led to further conclusion that on a microscopic level the tumors exhibit significant heterogeneity, including variation of stromal content and amount of adipose tissue. This heterogeneity exhibits itself in the spectral changes observed.

Meurens *et al.* compared FT-IR spectra with histomorphometry, a measurement of percent volume density of malignant cells in a tissue.[37] Seventy-five samples from 55 cases of breast carcinoma, that included invasive ductal carcinoma, lobular carcinoma, ductal carcinoma in situ and mucinous carcinoma, were studied in a macro transmission mode. They found that the most significant changes between malignant and "normal" tissues were observed at 1650, 1549, 1238, 1084 and $970\,cm^{-1}$. Correlation between morphometrical values and the IR values based on the different absorption bands led to a conclusion that phosphodiester groups in nucleic acids (1238 and $1084\,cm^{-1}$) and phosphate monoester groups of phosphorylated proteins and cellular nucleic acids ($970\,cm^{-1}$) are most closely related to the volume density of malignant cells. Ci *et al.*[54] studied 54 frozen tissue samples that were minced, dispersed and centrifuged. The cell suspension was eventually spread and allowed to dry to form a film. Samples included normal, hyperplasia, fibroadenoma and invasive ductal carcinoma examples. As in other studies, it was found that bands at 1338, 1280 and $1204\,cm^{-1}$ were weaker and broader while the band at $970\,cm^{-1}$ was sharper and stronger for carcinoma tissues. It was further found that the band near $1163\,cm^{-1}$ in benign tissues shifts to $1171\,cm^{-1}$ in carcinoma tissues and that the ratio of the absorbance of the bands at $\sim 1459\,cm^{-1}$ and $1239\,cm^{-1}$ is somewhat different for the four groups of tissues. They concluded that these differences reveal the differences in the relative contents of nucleic acids and collagen proteins in breast tissues.

It appears evident from these studies that analysis of breast tissues on a macroscopic level or even on a microscopic level, where the area analyzed is larger than the size of individual components, leads to "contamination" of spectra, or spectral averaging of all components present. These results then lead to conclusions as to the *nature of breast tissue and amount of connective tissue and/or nucleic acid present*. Although the results seem to be correlated with cancer, are they really a *detection* of cancer? Examination of histology of breast tissues would make it "obvious" that analysis of normal tissues would have more collagen/connective tissue spectral features and any spectral analysis, either intensity ratios or statistical analysis would be able to discriminate such spectra. It is important to emphasize that these statements are made in "hindsight" and would not be possible without the early studies discussed above because it is critical to understand exactly which components exhibit strong vibrational spectra.

We have tried to address the "contamination" question, combined with a desire to obtain spectra on "visible" pure components, i.e. stained tissues, by first employing a microscope with an ATR objective for measurement of stained tissues on glass slides[43] and more recently use of stained tissues on IR-reflective glass substrates and FPA detection.[47] As discussed above, the "main contamination" in the vibrational spectrum of a breast tissue comes from the spectrum of connective tissue and to a lesser extent from adipose tissue. Connective tissue composition varies throughout the body and includes epithelial basement membranes, networks of fibers and cellular components. The epithelial basement membrane is rich in type IV collagen, while the extracellular matrix is rich in type I, II and III collagen, elastin and proteoglycans. Type I is the most common type found, constituting 90% of the collagen in the body. Collagen, the major protein of connective tissue, contains approximately 33% glycine and 20–25% proline and hydroxyproline residues. The structure of collagen consists of three polypeptide chains wrapped around one another to form a three-fold superhelix with a right-handed twist, stabilized by intermolecular hydrogen bonding. Type I, II and III collagen molecules assemble

into ordered polymers, called collagen fibrils, which are long and thin, while type IV molecules do not form fibrils. An IR spectrum of collagen type I, measured in solid state using a single-bounce diamond ATR device, is shown in Figure 12(a). For comparison, the spectrum of connective tissue taken from a sample of normal breast tissue sample that is stained with H&E is shown in Figure 12(b). The spectrum of connective tissue is measured using a single-reflection diamond ATR accessory for which the spot size is 100 μm. The vibrational modes of collagen are assigned as follows: 1654 and 1634 cm^{-1} – amide I; 1544 cm^{-1} – amide II; 1450 and 1401 cm^{-1} – bending modes of methyl groups; 1337, 1280, 1237 and 1204 cm^{-1} – amide III and CH_2 wagging vibrations from glycine backbone and proline sidechains; 1082 and 1031 cm^{-1} – collagen carbohydrate residues. The similarity of the two spectra in Figure 12 leads to the conclusion that the major absorption bands observed in the connective tissue matrix of a breast tissue are due to collagen.

As discussed previously, FPA detection or use of synchrotron radiation allow for measurement at diffraction-limited spatial resolution. Studies are currently under way on a large number of patients to determine IR spectral features of individual components using FPA detection. To date, preliminary results indicate that IR spectra of epithelial cells (including nuclei and cytoplasm) in malignant tissues comprised of invasive ductal carcinoma are very similar, at least by visual comparison, to epithelial cells in normal tissues obtained from women who underwent a breast reduction mammoplasty surgical procedure. These results imply that changes in other components of a tissue other than epithelial cells might be more diagnostic of different states of breast diseases.

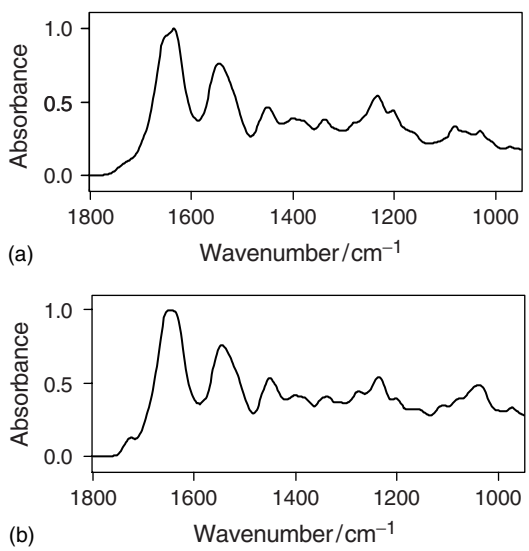

Figure 12. FT-IR absorbance spectrum of (a) collagen and (b) connective tissue (stroma) measured using single-bounce ATR accessory. Spot size is 100 μm. Spectra are normalized at $A_{1633} = 1.0$ for ease of comparison.

Most vibrational studies to date on breast tissues have been carried out with the goal of determining spectral features that can be correlated to cancer or any step in carcinogenesis. The early studies do appear to suggest that vibrational spectroscopy could be sensitive enough to confirm an absence of cancer or to detect the very early onset of disease for the 80% of women who undergo surgical biopsies because of abnormal mammography but do not have cancer. But once a pathologist confirms cancer, new questions arise: tumor grade, hormone receptor status, metastasis (both current and future), and effects of therapeutic intervention. Malins and colleagues[73–75,78] use isolated DNA from tissues for IR studies and have demonstrated that substantial differences are found in the spectra of DNA from women with normal and cancerous breast tissue.[73] More recently, they have shown that "metastatic tumor DNA is substantially more diverse than the tightly grouped non-metastatic tumor DNA"[74] and further that the "progression to the metastatic state involves structural modifications in DNA that are markedly different from the modifications associated with the formation of the primary tumor".[75] These studies imply not only that a new intervention can be designed but also that vibrational spectroscopy could be used to detect potential metastasis long before the physical event. Our preliminary studies, on a very tightly controlled group of patients in terms of age, receptor status, lymph node status and presence of her-2/neu oncogene showed very promising results of approximately 80% prediction on the development of metastasis. However, results were not as promising on an uncontrolled "blind" study and further investigation is in progress. Jackson *et al.*[48] have demonstrated, on a study of 77 breast tumors, and with the use of a multivariate pattern recognition technique, that tumors can be accurately classified by grade with 87% accuracy and by steroid receptor status with 93% accuracy. Preliminary data have also shown that the presence of metastasis in adjacent lymph nodes can be correctly predicted in about 75% of tumors.[123]

3.2 Cervix

Carcinoma of the cervix is one of the most preventable cancers that affect women, but yet women are still dying because the cancer is often caught too late. The US Department of Health and Human Services estimate that in the year 2001, 4600 American women will die from cervical cancer, and this number is much higher in third world countries where screening procedures are not in place. Worldwide, cervical cancer affects 500 000 women

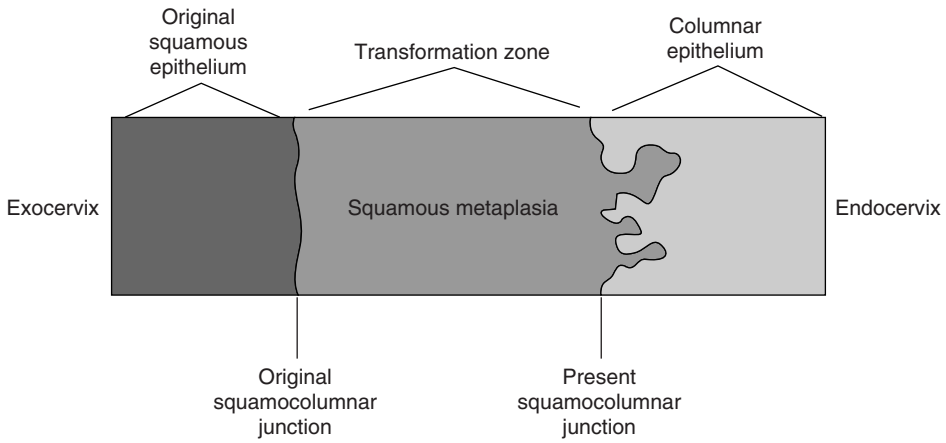

Figure 13. Schematic representation of the transformation zone and squamocolumnar junction.

annually, and after breast cancer, is the next most common malignancy found in women. On a more positive note, cervical cancer is only one of a few cancers with a well-established routine screening test, a Pap test. The Pap test was introduced as a cervical screening test in 1943 by Dr George Papanicolaou, after whom it is named. To obtain cervical cells, a speculum is inserted into the vagina so that the cervix and the vagina can be seen. A gentle cytobrush is inserted, via speculum, into the cervical opening to sample endocervical cells. Also, a small spatula is inserted through the speculum to gently scrape the ectocervix. The scraped cells are smeared, fixed and sent for an evaluation.

The cervix, also known as the neck of the uterus, is about 4 cm in length and 3 cm in diameter, and protrudes into the upper vagina. The exposed portion of the cervix, the *ectocervix*, is covered by an epithelial layer of cells that is 12–24 cells thick. This surface covering, called *squamous epithelium*, rests on a basement membrane beneath which are the deeper tissues that make up the substance of the cervix. The *endocervix*, the canal leading to the corpus (body of the uterus), is lined by mucosal ridges that contain mucinous columnar cells. The macroscopically visible junction between the ectocervix and the endocervix is known as the external os. The anatomic junction between the squamous and mucinous columnar epithelia is called the squamocolumnar junction. This junction undergoes many changes during a woman's life. The area between the original squamocolumnar junction and the new squamocolumnar junction is termed the "transformation zone", and is schematically shown in Figure 13. The most common form of cervical cancer, squamous cell carcinoma, occurs predominantly within the transformation zone. For most adequate Pap test screening, the specimen must contain both ectocervical (squamous) and endocervical (columnar) cells.

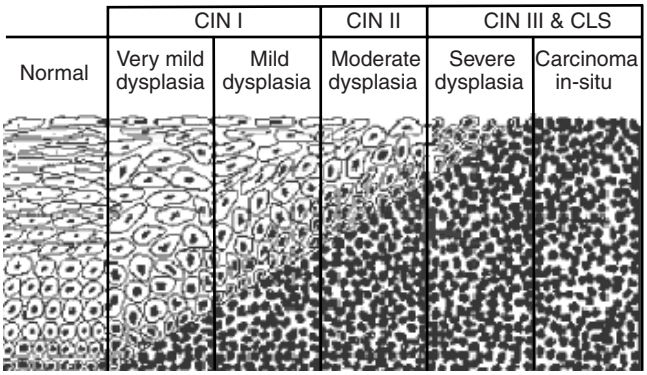

Figure 14. Schematic diagram of a squamous epithelium.

The cells of the surface squamous epithelium progress from round cells at the basement membrane to flat cells at the surface, as shown in Figure 14 (left panel). These cells are divided into four types: basal, parabasal, intermediate and superficial. The first layer, a monolayer of basal cells, is a parent of all other cells, being the only cell type in the epithelium capable of regeneration. As these cells rapidly divide, the daughter cells mature and migrate to the surface, and appear as several layers of parabasal cells. The division continues through the intermediate layer and ends at the superficial layer, with cells that easily shed. Basal cells are round and fairly small, about 10–12 μm in diameter, with a large nucleus and very little cytoplasm. Parabasal cells are typically 15–30 μm with a nucleus about 8–12 μm. Intermediate cells, 35–45 μm in diameter, are polygonal with a 10 μm nucleus. Superficial cells are flat, polyhedral in shape and are 40–50 μm in diameter with very small and dense nuclei, approximately 5–7 μm in diameter. During the maturation process, cells accumulate large amounts of glycogen. The concentration of glycogen increases towards the surface, with basal cells almost devoid of glycogen and superficial cells containing the highest concentration. The

concentration of glycogen is dependent on the hormone level during a woman's cycle and peaks close to ovulation. The relative number of intermediate and superficial cells also varies depending on the phase of the menstrual cycle.

A disorder of normal progression of cells is called a dysplasia, and is further classified as mild, moderate and severe depending on the thickness of epithelium that is affected. If the outermost cells look the same as those along the basement membrane, that disorder is called a CIS. It is believed that there is a progression from mild to moderate to severe dysplasia before developing CIS. If these dysplastic cells penetrate the basement membrane and invade into the deeper tissues then that is cancer. As with other cancers, cervical cancer is not one type of cancer but a number of different types, classified depending on the origin of the abnormal cells. Two types are most predominant: squamous cell carcinoma, which develops from the squamous epithelium, and adenocarcinoma, which arises from the glandular lining of the endocervical canal. Although over 80% of cervical cancer cases are squamous cell carcinomas, the incidence of adenocarcinoma of the cervix has increased 30% since 1973, despite a steep decline in squamous cell carcinoma. In part, this is due to "inability" of Pap smears to detect endocervical cells.[124] Currently, there are two reporting systems in use in the US with some modifications around the world: the Bethesda system and the CIN grading system. CIN stands for cervical intraepithelial neoplasia and implies an aberration in proliferation of cells. The Bethesda system uses a notation of squamous intraepithelial lesion (SIL) and changes are described as low-grade squamous intraepithelial lesion (LSIL) or high-grade squamous intraepithelial lesion (HSIL). Intraepithelial means that the abnormal cells are present only in the surface layer of cells. Spectroscopy papers often refer to one or the other system. Table 1 compares the various nomenclatures used to classify squamous cell abnormalities observed with the Pap test.

In the United States alone, 50 million Pap smear tests are performed every year and approximately 3.5 million Pap smears are classified as inconclusive. Worldwide the number is close to 110 million Pap tests performed annually with 7% indeterminate. The factors affecting the accuracy of Pap smears can be either clinically related or laboratory related and include, but are not limited to: contamination with blood or lubricants, inadequate sampling of the transformation zone, presence of infection, failure to identify dysplastic cells, poorly controlled technical process, and misinterpretation of diagnostic cells. The false negative rates (failure to identify abnormal cells) have been reported to be in the range of 1–80%, depending on the study, with the most frequently quoted average being 20%.[125,126] The false positive rates (detection of abnormal cells in a normal sample) have been reported to be as high as 32%.[127] The lesions missed most often by Pap smear test are either small lesions, advanced invasive lesions (due to infection and necrosis that can obscure true cytology), rapidly progressive lesions and the lesions located deep in the cervical canal. Women with inconclusive Pap smears are further tested for a human papillomavirus (HPV) infection and often undergo colposcopy, cervicography or biopsy. Other procedures can be used to check beneath the surface of the cervix, such as endocervical curettage, cone biopsy, or a dilation and curettage procedure. According to the US National Institutes of Health, HPV is found in virtually all cervical cancer cases worldwide. It is a known risk factor and is believed to be a cause of cervical cancer. Out of the more than 80 known types, more than 10 infect the genital tract, with HPV 16 and HPV 18 strains being most prevalent.[126] With many reports citing a fairly high occurrence of both false positive and false negative cases, combined with an enormous market potential, several adjunct tests to the Pap test have appeared over the last few years. Some tests address the laborious manual process of manual screening of smears, such as the PAPNET screening system (Neuromedical Systems, Inc., Suffern, NY), a system that uses neural network

Table 1. Classifications of squamous cell abnormalities

Description	Bethesda system	CIN grading	Class
Normal	Normal	Normal	Class I
Atypia, inflammation or neoplastic	ASCUS	Atypia	Class II
HPV	LSIL	HPV	Class II
Atypia with HPV	LSIL	Atypia, condylomatous atypia, koilocytic atypia	Class II
Mild dysplasia	LSIL	CIN I	Class III
Moderate dysplasia	HSIL	CIN II	Class III
Severe dysplasia	HSIL	CIN III	Class III
Carcinoma in-situ	HSIL	CIS	Class IV
Invasive cancer	Invasive cancer	Invasive cancer	Class V

Reproduced from http://www.oncolink.com

algorithms for identification of abnormal cells among all cells on a smear. Other new tests, such as the ThinPrep processor (Cytyc Corporation, Marlborough, MA, USA) address "artifacts" in a smear slide preparation by offering an automated system that takes cells collected in a fluid suspension and prepares a microscope slide with an evenly dispersed layer of cells. Preparation of slides with the ThinPrep technique was found to be superior to the conventional preparation in the detection of low-grade squamous intraepithelial abnormalities.[128] Additionally, ThinPrep may be more accurate than the traditional Pap smear in detecting endocervical cells.[124]

Many vibrational spectroscopy studies, beginning with the work of Wong and colleagues, have concentrated on studies of Pap smear samples for "early detection of cancer", rather than cervical biopsies. In a Pap test, a heterogeneous mixture of cells, originating from different layers of a cervical tissue, is sampled. This mixture of cervical cells is also known as exfoliated cells. The first papers on FT-IR studies of exfoliated cervical cells and cervical tissues in the early 1990s from the group of Wong and colleagues found several spectral differences in malignant as compared to normal cells and tissues.[28,56] The spectroscopic differences included changes in intensity of bands at 1303, 1244, 1155, 1082, 1047 and 1025 cm^{-1}; shift of peaks at 1244, 1155 and 1082 cm^{-1}; and appearance of the band at 970 cm^{-1}. The ratio of intensities of the band due to glycogen at 1025 cm^{-1} (Figure 4) to the band due to nucleic acids at 1082 cm^{-1} band was found to differ between malignant and normal cells. They also noted that spectra of the dysplastic cells were intermediate in magnitude between the spectra of normal and malignant cells, and that the frequency of the 1082 cm^{-1} was not shifted to higher frequencies, as for malignant samples. It was concluded that in malignant cells and tissues, the amount of glycogen is dramatically decreased, significant increases occur in hydrogen bonding of phosphodiester groups of nucleic acids, a loss of C–OH groups of proteins takes place, and a greater disorder occurs in the conformation and orientation of the methylene chains of membrane lipids. The glycogen level decreases during carcinogenesis, so decreases in intensity of the bands at 1155 and 1023–1025 cm^{-1}, which are due to absorption of glycogen, are consistent. Yazdi *et al.*[59] studied cervical samples from 133 women and concluded that changes in the IR spectra are also clearly observed in cervical cells from preinvasive lesions and other conditions such as benign cellular changes. Although confirming that FT-IR spectra of abnormal cervical samples are different from the spectra of normal samples, it was shown that it is the HSIL specimens (95% of samples) that exhibited the most dramatic differences in the IR spectra, and that only 54% of LSIL cases and 33% of ASCUS (atypical squamous cells of undetermined significance) cases exhibited significant spectral changes. These observations were considered to be due to heterogeneity of lesions classified as LSIL and ASCUS. Fung *et al.*[61] compared FT-IR spectroscopy in screening of cervical cells with conventional Pap smears using colposcopy directed biopsy as a gold standard. Exfoliated cervical cells from 301 patients were collected. The positive IR spectra were characterized by several or all changes in the spectra described above. The sensitivity and specificity were 86.6 and 90.5% for Pap smears and 98.6% and 98.8% for FT-IR. The Pap test showed 13.4% false negative, 9.5% false positive, compared to FT-IR spectroscopy that showed 1.4% false negative and 1.2% false positive.

Wood *et al.*[60] investigated use of PCA for data reduction and analysis. In a study of 272 patients, the observed spectra were visually sorted into two profiles: type 1 and type 2. Type 1 spectra exhibited a profile characteristic of normal epithelial cells with intense glycogen bands at 1022 and 1150 cm^{-1}, and a pronounced phosphate stretch at 1078 cm^{-1}. Type 2 spectra exhibited features characteristic of malignant cells, with pronounced nucleic acids bands and a reduction in intensity of glycogen band, similar to those described by Wong. Spectra of cultured malignant cells (from HeLa cell lines) exhibited a number of features common with type 2 spectra. PCA decomposition resulted in a score plot that showed general separation of the visually categorized spectra. Eighty-six percent of the spectra that exhibited type 1 profile by visual sorting and PCA analysis of FT-IR spectra were diagnosed normal by Pap smear and 87% exhibiting type 2 spectral profile were diagnosed abnormal. Cohenford and colleagues,[62] in a study of 436 patients, also demonstrated the application of PCA to a study of cervical smears and suggested that blood may be an interfering substance. They found a sensitivity of 79% and specificity of 77%. The FT-IR spectra discussed above in the early work of Wong's group and others were collected in a macro transmission mode, in most cases using diamond anvil cells with pressure dependence. Although specimens containing scraped exfoliated cells should not have much surrounding material except cells, as other studies came to light it became clear that other factors could be contributing to spectral changes observed. Shaw *et al.*[67] showed that IR spectra of exfoliated cells carry information regarding the presence of dysplasia but concluded that automated feature extraction and pattern recognition methods are required to distinguish IR spectra of dysplastic smears from normal.

In 1998, Diem and colleagues demonstrated in a series of papers[40,64] that FT-IR spectroscopy could be used as a tool to monitor maturation and differentiation of human cervical cells[40] and compared spectra of biopsies of squamous epithelia to exfoliated cervical cells.[64] They further compared columnar tissue with squamous epithelium[38] and

found that the spectra observed for columnar cells in tissue samples were also detected in the spectra of exfoliated cells, indicating the presence of endocervical cells. It was shown that the columnar or glandular cells exhibit spectral features similar to those observed for pure cervical mucus. All four different layers in epithelial tissue and the stroma exhibit IR spectra distinguishable from each other. It was further concluded that spectral features of healthy cervical cells are dominated by spectral features of glycogen and proteins and that nucleic acids do not seem to contribute, especially in the case of fully mature cervical cells. A hypothesis was put forward that in a mature cervical cell the nucleus is opaque or nearly opaque in the mid-infrared range, and that nucleic acid spectral features were due to RNA in cytoplasm, and not the DNA in the nucleus. This hypothesis was "verified" by an experiment in which an IR beam of ca. 5 μm diameter and focused on a cell nucleus produced no IR light while a similar sized beam, focused on cytoplasm, produced a weak but an observable spectrum. It was also concluded, based on the spectra of single exfoliated cells, that the glycogen concentration of single, mature cells can vary tremendously. Comparison of samples from different patients led to the conclusion that spectra are often contaminated by blood components (leukocytes and red blood cells), fungi or mucous. Similar conclusions were reached by Wood *et al.*[129] that bacteria, yeast, mucins, semen and other contaminants might contaminate FT-IR spectra of smears. In paper four of a series of papers from Diem's group[44] it was observed that cells found at the surface of dysplastic tissue had spectral characteristics of basal cells. As disease progressed toward cancer, a loss of spectral detail was observed in the low frequency DNA triad of peaks. The presence of spectral characteristics attributed to basal cells could serve as an indicator of dysplasia given that basal cells are rarely found in normal exfoliated cervical smears.

Cohenford and Rigas[63] using FT-IR microspectroscopy examined individual cervical cells from normal, dysplastic, and malignant samples. Cervical scrapings were processed using a Cytyc ThinPrep processor, which filters out mucus and debris and spreads the cells uniformly on a microscope slide. Samples were collected from 22 women and over 2000 cells were analyzed. Ninety-five percent of normal exfoliated cells, comprised overwhelmingly from superficial and intermediate cells, displayed two distinct spectral patterns, designated A and B, while the remaining 5% displayed an intermediate pattern. Three main differences exist between the two patterns of spectra. Compared with pattern A, in pattern B the amplitude of the band peaking around 1027 cm^{-1} is dramatically reduced; the 1105 and 1153 cm^{-1} peaks are shifted toward higher wavenumber; and the peak intensity ratio 1080 cm^{-1} to the amide II is dramatically reduced. The following conclusions were reached: (1) superficial and intermediate squamous cervical cells exhibit no spectral difference; (2) both cell types display three distinct spectral patterns – A, B and an intermediate pattern; (3) spectra of cytologically normal cells from dysplastic or malignant cervical cells differ significantly from the spectra of cytologically normal cells from normal samples; and (4) parabasal, endocervical, koilocytic, dysplastic and malignant cells showed pattern B spectra. These findings suggest that "the structural changes underlying the spectroscopic changes are involved in or are a product of cervical carcinogenesis" and "the neoplastic process may be more extensive than currently recognized with morphological criteria".

As discussed above, it has become apparent over the past few years that spectral differences observed in exfoliated cell smears or cervical tissues that might be due to the onset of carcinogenesis are also due to other processes or the presence of other material. Many groups are taking a step back to investigate possible effects of cell division, cyclical change,[130] presence of HIV infection,[68] HPV virus,[131] and the presence of contaminants such as blood constituents, semen, mucin, inflammation, and other possible cellular and noncellular components. Near-infrared[58] and near-infrared Raman[88,117] spectroscopies have been used for the study of cervical cells and tissues with similar results and challenges as discussed for mid-infrared studies above.

4 CONCLUSIONS

"Vibrational Spectroscopy in the Detection of Cancer", as a technique to be used and accepted by the medical community is still in its early stages. Although we emphasized pitfalls and urged caution throughout the article, we remain optimistic that vibrational spectroscopy will find its place somewhere along the line of this dreadful disease. And finding the "right place" in that line is important. That knowledge will only come from merging of the fields – collaborations with doctors and pathologists is a necessity. Confirmation of a cancer on a tissue biopsy might not be much of a need depending on the cancer but help with prognosis and treatment (monitoring of therapeutic intervention) is a dream for oncologists. Spectroscopy seems to be ideally suited for screening procedures. It is inexpensive, can be automated, the measurements are fast and instruments are fairly inexpensive. As an example, screening of Pap smears offers a tremendous market potential and there is a need for an automated system. So the desire is strong but are we ready? In general, for most cancers, more research is needed. We urge patience and a quest for understanding the morphology and biology of the sample before

proceeding with spectroscopy. And we also urge spectroscopists to take a step back and look more carefully at their spectra – they are full of invaluable information that is waiting to be interpreted and understood at the cellular level.

ACKNOWLEDGMENTS

I would like to thank the following people: Curt Marcott and Gloria Story from Procter and Gamble, my collaborators on breast cancer imaging project for the tremendous amount of work that has been done over the last couple of years, and Curt for reading and editing the manuscript; Dr Beth Johnson, Director of Pathology at Central DuPage Hospital, for her patience with my ideas, for teaching me to "understand" what it is I see through the microscope and for providing guidance and samples over many years; Larry Nafie for editorial corrections; Jan Kubelka and Tim Keiderling for providing Raman spectra of proteins; Max Diem for providing the spectrum of a lipid; Larry Carr and Bob Messerschmidt for fruitful discussions; management at Vysis for allowing me to explore and all spectroscopists in this field for all their efforts, determination and desire to succeed, for sharing ideas and results and for believing.

This article is dedicated to the memory of my father-in-law, Abram Dukor, who at the age of 60 bravely fought the battle of cancer but did not win the war.

ABBREVIATIONS AND ACRONYMS

ASCUS	Atypical Squamous Cells of Undetermined Significance
CIN	Cervical Intraepithelial Neoplasia
CIS	Carcinoma In-situ
DCIS	Ductal Carcinoma In-situ
FDA	US Food and Drug Administration
FOV	Field-of-view
H&E	Hematoxylin and Eosin
HPV	Human Papillomavirus
HSIL	High-grade Squamous Intraepithelial Lesion
IRE	Internal Reflection Element
LCIS	Lobular Carcinoma In-situ
LRS	Least Resolvable Separation
LSIL	Low-grade Squamous Intraepithelial Lesion
MRI	Magnetic Resonance Imaging
NSLS	National Synchrotron Light Source
SIL	Squamous Intraepithelial Lesion
UV	Ultraviolet

REFERENCES

1. A. Elliott and E.J. Ambrose, *Nature*, **165**, 921 (1950).
2. E.Q. Blout and M.J. Fields, *Biol. Chem.*, **178**, 335 (1949).
3. W.K. Surewicz and H.H. Mantsch, 'Infrared Absorption Methods for Examining Protein Structure', in "Spectroscopic Methods for Determining Protein Structure in Solution", ed. H.A. Havel, VCH Publishers, New York, 135 (1996).
4. L.G. Tensmeyer and E.W. Kauffman II, 'Protein Structure as Revealed by Nonresonance Raman Spectroscopy', in "Spectroscopic Methods for Determining Protein Structure in Solution", ed. H.A. Havel, VCH Publishers, New York, 69 (1996).
5. P. Pancoska, J. Kubelka and T.A. Keiderling, *Appl. Spectrosc.*, **53**, 655 (1999).
6. M. Tsuboi, 'Application of Infrared Spectroscopy to Structure Studies of Nucleic Acids', in "Applied Spectroscopy Reviews", ed. E.G. Brame, Jr, Marcel Dekker, New York, 45, Vol. 3 (1969).
7. J. Liquier and E. Taillandier, 'Infrared Spectroscopy of Nucleic Acids', in "Infrared Spectroscopy of Biomolecules", eds H.H. Mantsch and D. Chapman, Wiley-Liss, New York, 131 (1996).
8. R.N.A.H. Lewis and R.N. Mcelhaney, 'Fourier Transform Infrared Spectroscopy in the Study of Hydrated Lipids and Lipid Bilayer Membranes', in "Infrared Spectroscopy of Biomolecules", eds H.H. Mantsch and D. Chapman, Wiley-Liss, New York, 159 (1996).
9. K. Brandenburg and U. Seydel, 'Fourier Transform Infrared Spectroscopy of Cell Surface Polysaccharides', in "Infrared Spectroscopy of Biomolecules", eds H.H. Mantsch and D. Chapman, Wiley-Liss, New York, 203 (1996).
10. B. Alberts, D. Bray, J. Lewis, M. Raff, K. Roberts and J.D. Watson (eds), 'Molecular Biology of the Cell', Garland Publishing, New York (1983).
11. L.A.G. Ries, C.L. Kosary, B.F. Hankey, B.A. Miller, L. Clegg and B.K. Edwards (eds), 'SEER Cancer Statistics Review, 1973–1996', National Cancer Institute, Bethesda, MD (1999).
12. D. Sheehan, 'Theory and Practice of Histotechnology', C.V. Mosby, St. Louis (1980).
13. E.B. Hanlon, R. Manoharan, T.-W. Koo, K.E. Shafer, J.T. Motz, M. Fitzmaurice, J.R. Kramer, I. Itzkan, R.R. Dasari and M.S. Feld, *Phys. Med. Biol.*, **45**, R1 (2000).
14. E. Benedetti, F. Papineschi, P. Vergamini, R. Consolini and G. Spremolla, *Leukemia Res.*, **8**, 483 (1984).
15. R.A. Shaw, M. Leroux, M. Paraskevas, F.B. Guijon, S. Kotowich and H.H. Mantsch, 'Discrimination and Quantitation using IR Spectra: Novel Methods for Serum Analysis and for Servical Dysplasia Screening', in "Infrared Spectroscopy: New Tool in Medicine", eds H.H. Mantsch and M. Jackson, SPIE, Washington, DC, 42, Vol. 3257 (1998).
16. G.H. Werner, J. Früh, F. Keller, H. Greger, R. Somorjai, B. Dolenko, M. Otto and D. Böcker, 'Mid-infrared Spectroscopy as Tool for Disease Pattern Recognition from

Human Blood', in "Infrared Spectroscopy: New Tool in Medicine", eds H.H. Mantsch and M. Jackson, SPIE, Washington, 35, Vol. 3257 (1998).

17. A.J. Berger, T.-W. Koo, I. Itzkan, G. Horowitz and M.S. Feld, *Appl. Opt.*, **38**, 2916 (1999).
18. S.Yu. Venyaminov and F.G. Prendergast, *Anal. Biochem.*, **248**, 234 (1997).
19. P.S. Shah, F. Bizik, R.K. Dukor and P.K. Qasba, *Biochim. Biophys. Acta*, **1480**, 222 (2000).
20. H.H. Eysel, M. Jackson, A. Nikhulin, R.L. Somorjai, G.T.D. Thomson and H.H. Mantsch, *Biospectroscopy*, **3**, 161 (1997).
21. M. Jackson and H.H. Mantsch, 'Ex-vivo Tissue Analysis by Infrared Spectroscopy', in "Encyclopedia of Analytical Chemistry", ed. R.A. Meyers, Wiley, Chichester, 131–156 (2000).
22. P.R. Griffiths and J.A. de Heseth, 'Fourier Transform Infrared Spectrometry', Wiley-Interscience, New York (1986).
23. E.K. Blout and R.C. Mellors, *Science*, **110**, 137 (1949).
24. T.J. O'Leary and I.W. Levin, *Lab. Invest.*, **53**, 240 (1985).
25. T.J. O'Leary, W.F. Engler and K.M. Venture, *Appl. Spectrosc.*, **43**, 1095 (1989).
26. B. Rigas, S. Morgello, I.S. Goldman and P.T.T. Wong, *Proc. Natl. Acad. Sci. USA*, **87**, 8140 (1990).
27. P.T.T. Wong and B. Rigas, *Appl. Spectrosc.*, **44**, 1715 (1990).
28. P.T.T. Wong, R.K. Wong and M.F.K. Fung, *Appl. Spectrosc.*, **47**, 1058 (1993).
29. P.T.T. Wong, S.M. Goldstein, R.C. Grekin, T.A. Godwin, C. Pivik and B. Rigas, *Cancer Res.*, **53**, 762 (1993).
30. P.T.T. Wong, S. Lacelle and H.M. Yazdi, *Appl. Spectrosc.*, **47**, 1830 (1993).
31. S.M. LeVine and D.L. Wetzel, *Am. J. Pathol.*, **145**, 1041 (1994).
32. M. Jackson, L.-P. Choo, P.H. Watson, W.C. Halliday and H.H. Mantsch, *Biochim. Biophys. Acta*, **1270**, 1 (1995).
33. H. Fabian, M. Jackson, L. Murphy, P.H. Watson, I. Fichtner and H.H. Mantsch, *Biospectroscopy*, **1**, 37 (1995).
34. L.-S. Lee, S.-Y. Lin, C.-W. Chi, H.-C. Liu and C.-L. Cheng, *Cancer Lett.*, **94**, 65 (1995).
35. K.Z. Liu, M. Jackson, M.G. Sowa, H. Ju, I.M.C. Dixon and H.H. Mantsch, *Biochim. Biophys. Acta*, **1315**, 73 (1996).
36. M.F.K. Fung, M.K. Senterman, N.Z. Mikhael, S. Lacelle and P.T.T. Wong, *Biospectroscopy*, **2**, 155 (1996).
37. M. Meurens, J. Wallon, J. Tong, H. Noël and J. Haot, *Vib. Spectrosc.*, **10**, 341 (1996).
38. L. Chiriboga, P. Xie, W. Zhang and M. Diem, *Biospectroscopy*, **3**, 253 (1997).
39. D.M. Haaland, H.D.T. Jones and E.V. Thomas, *Appl. Spectrosc.*, **51**, 340 (1997).
40. L. Chiriboga, P. Xie, H. Yee, V. Vigorita, D. Zarou, D. Zakim and M. Diem, *Biospectroscopy*, **4**, 47 (1998).
41. M. Jackson, B. Ramjiawan, M. Hewko and H.H. Mantsch, *Cell. Mol. Biol.*, **44**, 89 (1998).
42. P. Lasch and D. Naumann, *Cell. Mol. Biol.*, **44**, 189 (1998).
43. R.K. Dukor, M.N. Liebman and B.L. Johnson, *Cell. Mol. Biol.*, **44**, 211 (1998).
44. L. Chiriboga, P. Xie, H. Yee, D. Zarou, D. Zakim and M. Diem, *Cell. Mol. Biol.*, **44**, 219 (1998).
45. H. Fabian, R. Wessel, M. Jackson, A. Schwartz, P. Lasch, I. Fichtner, H.H. Mantsch and D. Naumann, 'IR-spectroscopy and IR-microscopy of Human Breast Tumors, Xenografted Breast Tumors, and Breast Tumor Cell Lines', in "Infrared Spectroscopy: New Tool in Medicine", eds H.H. Mantsch and M. Jackson, SPIE, Washington, DC, 13, Vol. 3257 (1998).
46. L.M. McIntosh, J.R. Mansfield, A.N. Crowson, H.H. Mantsch and M. Jackson, *Biospectroscopy*, **5**, 265 (1999).
47. R.K. Dukor, G.M. Story and C. Marcott, 'A Method for Analysis of Clinical Tissue Samples using FT-IR Microspectroscopic Imaging', in "Spectroscopy of Biological Molecules: New Directions", eds J. Greve, G.J. Puppels and C. Otto, Kluwer Academic Publishers, Norwell, MA, 471 (1999).
48. M. Jackson, J.R. Mansfield, B. Dolenko, R.L. Somorjai, H.H. Mantsch and P.H. Watson, *Cancer Detect. and Prevent.*, **23**, 245 (1999).
49. P. Lasch, E.N. Lewis, L.H. Kidder and D. Naumann, *Proc. SPIE*, **3920**, 129 (2000).
50. M. Diem, L. Chiriboga and H. Yee, *Biopolymers:Biospectroscopy*, **57**, 282 (2000).
51. K. Yano, S. Ohoshima, Y. Gotou, K. Kumaido, T. Moriguchi and H. Katayama, *Anal. Biochem.*, **287**, 218 (2000).
52. K. Yano, S. Ohoshima, Y. Shimizu, T. Moriguchi and H. Katayama, *Cancer Lett.*, **110**, 29 (1996).
53. S. Takahashi, A. Satomi, K. Yano, H. Kawase, T. Tanimizu, Y. Tuji, S. Murakami and R. Hirayama, *J. Gastroenterol.*, **34**, 474 (1999).
54. Y.X. Ci, T.Y. Gao, J. Feng and Z.Q. Guo, *Appl. Spectrosc.*, **53**, 312 (1999).
55. P.T.T. Wong, E.D. Papavassiliou and B. Rigas, *Appl. Spectrosc.*, **45**, 1563 (1991).
56. P.T.T. Wong, R.K. Wong, T.A. Caputo, T.A. Godwin and B. Rigas, *Proc. Natl. Acad. Sci. USA*, **88**, 10 988 (1991).
57. P.T.T. Wong, S. Lacelle, M.F.K. Fung and S. Senterman, *Biospectroscopy*, **1**, 357 (1995).
58. Z. Ge, C.W. Brown and H.J. Kisner, *Appl. Spectrosc.*, **49**, 432 (1995).
59. H.M. Yazdi, M.A. Bertrand and P.T.T. Wong, *Acta Cytologica*, **40**, 664 (1996).
60. B.R. Wood, M.A. Quinn, F.R. Burden and D. McNaughton, *Biospectroscopy*, **2**, 143 (1996).
61. M.F.K. Fung, M. Senterman, P. Eid, W. Faught, N.Z. Mikhael and P.T.T. Wong, *Gynecol. Oncol.*, **66**, 10 (1997).
62. M.A. Cohenford, T.A. Godwin, F. Cahn, P. Bhandare, T.A. Caputo and B. Rigas, *Gynecol. Oncol.*, **66**, 59 (1997).
63. M.A. Cohenford and B. Rigas, *Proc. Natl. Acad. Sci. USA*, **95**, 15 327 (1998).

64. L. Chiriboga, P. Xie, V. Vigorita, D. Zarou, D. Zakim and M. Diem, *Biospectroscopy*, **4**, 55 (1998).
65. S.R. Lowry, *Cell. Mol. Biol.*, **44**, 169 (1998).
66. M. Romeo, F. Burden, M. Quinn, B. Wood and D. McNaughton, *Cell. Mol. Biol.*, **44**, 179 (1998).
67. R.A. Shaw, F.B. Guijon, M. Paraskevas, S.L. Ying and H.H. Mantsch, *Anal. Quantitat. Cytol. Histol.*, **21**, 292 (1999).
68. B. Rigas, K. LaGuardia, L. Qiao, P.S. Bhandare, T. Caputo and M.A. Cohenford, *J. Lab. Clin. Med.*, **135**, 26 (2000).
69. E. Benedetti, L. Teodori, M.L. Trinca, P. Vergamini, F. Salvati, F. Mauro and G. Spremolla, *Appl. Spectrosc.*, **44**, 1276 (1990).
70. B. Rigas and P.T.T. Wong, *Cancer Res.*, **52**, 84 (1992).
71. C.P. Schultz, K.-Z. Liu, J.B. Johnston and H.H. Mantsch, *J. Mol. Struct.*, **408/409**, 253 (1997).
72. S. Boydston-White, T. Gopen, S. Houser, J. Bargonetti and M. Diem, *Biospectroscopy*, **5**, 219 (1999).
73. D.C. Malins, N.L. Polissar, K. Nishikida, E.H. Holmes, H.S. Gardner and S.J. Gunselman, *Cancer*, **75**, 503 (1995).
74. D.C. Malins, N.L. Polissar and S.J. Gunselman, *Proc. Natl. Acad. Sci. USA*, **93**, 2557 (1996).
75. D.C. Malins, N.L. Polissar and S.J. Gunselman, *Proc. Natl. Acad. Sci. USA*, **93**, 14 047 (1996).
76. D.C. Malins, N.L. Polissar and S.J. Gunselman, *Proc. Natl. Acad. Sci. USA*, **94**, 259 (1997).
77. G.I. Dovbeshko and N.Ya. Gridina, 'IR Spectroscopic Studies of Tumor DNA', in "Spectroscopy of Biological Molecules: Modern Trend", eds P. Carmona, R. Navarro and A. Hernanz, Kluwer Academic Publishers, Norwell, MA, 451 (1997).
78. D.C. Malins, N.L. Polissar, S. Schaefer, Y. Su and M. Vinson, *Proc. Natl. Acad. Sci. USA*, **95**, 7637 (1998).
79. Q. Peng, R.D. Soloway, J.-G. Wu, X.S. Zhou, D.W. Zhao, D.F. Xu, W. Fu and S.F. Wang, Abstract for the American Gastroenterological Association and American Association for the Study of Liver Diseases, May 19–22 (1996).
80. N.I. Afanasyeva, 'Diagnostics of Normal and Cancer Tissues by Fiberoptic Evanescent Wave Fourier-transform IR (FEW-FT-IR) Spectroscopy', in "AIP Conference Proceedings, 11th International Conference on Fourier Transform Spectroscopy", ed. J.A. de Haseth, American Institute of Physics, Woodbury, NY, 290–293 (1998).
81. J.-G. Wu, *Biopolymers:Biospectroscopy*, in press.
82. S.B. Schwab and R.L. McCreery, *Anal. Chem.*, **56**, 2199 (1984).
83. C.J. Frank, D.C.B. Redd, T.S. Gansler and R.L. McCreery, *Anal. Chem.*, **66**, 319 (1994).
84. C.J. Frank and R.L. McCreery, *Anal. Chem.*, **67**, 777 (1995).
85. G.J. Puppels, T. van Aken, R. Wolthuis, P.J. Caspers, T.C. Bakker Schut, H.A. Bruining, T.J. Römer, H.P.J. Buschman, M.L. Wach and J.S. Robinson, Jr, 'In vivo Tissue Characterization by Raman Spectroscopy', in "Infrared Spectroscopy: New Tool in Medicine", eds H.H. Mantsch and M. Jackson, SPIE, Washington, DC, 78, Vol. 3257 (1998).
86. H.P.J. Buschman, T. van Aken, E.T. Marple, A. van der Laarse, A.V.G. Bruschke and G.J. Puppels, 'In Vivo Raman Spectroscopy During Laparoscopy', in "Spectroscopy of Biological Molecules: New Directions", eds J. Greve, G.J. Puppels and C. Otto, Kluwer Academic Publishers, Norwell, MA, 483 (1999).
87. J.F. Brennan, Y. Wang, R.R. Dasari and M.S. Feld, *Appl. Spectrosc.*, **51**, 201 (1997).
88. A. Mehadevan-Jansen, M.F. Mitchell, N. Ramanujam, U. Utzinger and R. Richards-Kortum, *Photochem. Photobiol.*, **68**, 427 (1998).
89. R.H. Clarke, E.B. Hanlon, J.M. Isner and H. Brody, *Appl. Opt.*, **26**, 3175 (1987).
90. R.R. Alfano, C.H. Liu, W.L. Sha, H.R. Zhu, D.L. Atkins, J. Cleary, R. Prudente and E. Clemer, *Lasers Life Sci.*, **42**, 23 (1991).
91. R.P. Rava, J.J. Baraga and M.S. Feld, *Spectrochim. Acta A*, **47**, 509 (1991).
92. A. Mizuno, T. Hayashi, K. Tashibu, S. Maraishi, K. Kawauchi and Y. Ozaki, *Neurosci. Lett.*, **141**, 47 (1992).
93. J.J. Baraga, M.S. Feld and R.P. Rava, *Appl. Spectrosc.*, **46**, 187 (1992).
94. R. Manoharan, Y. Wang and M.S. Feld, *Spectrochim. Acta A*, **52**, 215 (1996).
95. M.G. Shim and B.C. Wilson, *J. Raman Spectrosc.*, **28**, 131 (1997).
96. P.J. Caspers, G.W. Lucassen, R. Wolthuis, H.A. Bruining and G.J. Puppels, *Biospectroscopy*, **4**, S31 (1998).
97. R.G. Messerschmidt and M.A. Harthcock (eds), 'Infrared Microspectroscopy: Theory and Applications', Marcel Dekker, New York (1988).
98. R.G. Messerschmidt, 'Minimizing Optical Nonlinearities in Infrared Microspectroscopy', in "Practical Guide to Infrared Microspectroscopy", ed. H.J. Humecki, Marcel Dekker, New York, 3 (1995).
99. J.A. Reffner and P.A. Martoglio, 'Uniting Microscopy and Spectroscopy', in "Practical Guide to Infrared Microspectroscopy", ed. H.J. Humecki, Marcel Dekker, New York, 41 (1995).
100. D.L. Wetzel and S.M. LeVine, 'Biological Applications of Infrared Microspectroscopy', in "Infrared and Raman Spectroscopy of Biological Materials", eds H.U. Gremlich and B. Yans, Marcel Dekker, New York, 101–142 (2001).
101. B.K. Johnson, 'Optics and Optical Instruments', Dover Publications Inc., New York (1960).
102. R.G. Messerschmidt, personal communication.
103. G.L. Carr, *Rev. Sci. Instrum.*, **72**, 1 (2001).
104. G.L. Carr, O. Merlo, M. Munsli, S. Springer and S.C. Ho, *Proc. SPIE*, **3775**, 22 (1999).
105. G.L. Carr, personal communication.
106. N. Jamin, P. Dumas, J. Moncuit, W.-H. Fridman, J.-L. Teillaud, G.L. Carr and G.P. Williams, *Proc. Natl. Acad. Sci. USA*, **95**, 4837 (1998).
107. H.-Y.N. Holman, M.C. Martin, E.A. Blakely, K. Bjornstad and W.R. McKinney, *Biopolymers: Biospectroscopy*, **57**, 329 (2000).

108. E.N. Lewis, P.J. Treado, R.C. Reeder, G.M. Story, A.E. Dowrey, C. Marcott and I.W. Levin, *Anal. Chem.*, **67**, 3377 (1995).

109. E.N. Lewis, A.M. Gorbach, C. Marcott and I.W. Levin, *Appl. Spectrosc.*, **50**, 263 (1996).

110. C. Marcott, R.C. Reeder, E.P. Paschalis, D.N. Tatakis, A.L. Boskey and R. Mendelsohn, *Cell. Mol. Biol.*, **1**, 109 (1998).

111. M.G. Shim and B.C. Wilson, *Photochem. Photobiol.*, **63**, 662 (1996).

112. A. Mizuno, H. Kitajima, K. Kawauchi, S. Maraishi and Y. Ozaki, *J. Raman Spectrosc.*, **25**, 265 (1994).

113. S. Keller, B. Schrader, A. Hoffman, W. Schrader, K. Metz, A. Rehlaender, J. Pahnke, M. Ruwe and W. Budach, *J. Raman Spectrosc.*, **25**, 663 (1994).

114. D.C.B. Redd, Z.C. Feng, K.T. Yue and T.S. Gansler, *Appl. Spectrosc.*, **47**, 787 (1993).

115. R. Manoharan, K. Shafer, L. Perelman, J. Wu, K. Chen, G. Deinum, M. Fitzmauice, J. Myles, J. Crowe, R.R. Dasari and M.S. Feld, *Photochem. Photobiol.*, **67**, 15 (1998).

116. R. Manoharan, Y. Wang, R.R. Dasari, S. Singer, R.P. Rava and M.S. Feld, *Lasers Life Sci.*, **6**, 217 (1995).

117. A. Mehadevan-Jansen, M.F. Mitchell, N. Ramanujam, A. Malpica, S. Thompsen, U. Utzinger and R. Richards-Kortum, *Photochem. Photobiol.*, **68**, 123 (1998).

118. L. Chiriboga, H. Yee and M. Diem, *Appl. Spectrosc.*, **54**, 480 (2000).

119. B.W. Barry, H.G.M. Edwards and A.C. Williams, *J. Raman Spectrosc.*, **23**, 641 (1992).

120. A.C. Williams, B.W. Barry, H.G. Edwards and D.W. Farwell, *Pharm. Res.*, **10**, 1642 (1993).

121. S. Fendel and B. Schrader, *Fresenius' J. Anal. Chem.*, **360**, 609 (1998).

122. M. Gniadecka, N.O. Faurskov, D.H. Christensen and H.C. Wulf, *J. Invest. Dermatol.*, **110**, 393 (1998).

123. M. Jackson and H.H. Mantsch, *J. Mol. Struct.*, **408/409**, 105 (1997).

124. H.O. Smith, M.F. Tiffany, C.R. Qualls and C.R. Key, *Gynecol. Oncol.*, **78**, 97 (2000).

125. H.J. Soost, H.J. Lange, W. Lehmacher and B. Ruffing-Kullmann, *Acta Cytol.*, **35**, 8 (1991).

126. US Preventative Services Task Force, 'Screening for Cervical Cancer', in "Guide to Clinical Preventive Services", 2nd edition, US Department of Health and Human Services, Washington, DC (1996).

127. M.T. Fahey, L. Irwig and P. Macaskill, *Am. J. Epidemol.*, **141**, 680 (1995).

128. K.R. Lee, R. Ashfaq, G.G. Birdsong, M.E. Corkill, K.M. McIntosh and S.L. Inhorn, *Obstet. Gynecol.*, **90**, 278 (1997).

129. B. Wood, M. Quinn, B. Tait, M. Ashdown, T. Hislop, M. Romeo and D. McNaughton, *Biospectroscopy*, **4**, 75 (1998).

130. M.J. Romeo, B.R. Wood and D. McNaughton, *Vib. Spectrosc.*, in press (2001)

131. B.J. Morris, C. Lee, B.N. Nightingale, E. Molodysky, M.J. Morris and R. Appio, *Gynecol. Oncol.*, **66**, 59 (1997).